



OPEN

# Removing unwanted variation from large-scale RNA sequencing data with PRPS

Ramyar Molania<sup>1,2</sup> , Momeneh Foroutan<sup>3</sup>, Johann A. Gagnon-Bartsch<sup>4</sup>, Luke C. Gandolfo<sup>1,2,5</sup>, Aryan Jain<sup>1</sup> , Abhishek Sinha<sup>1</sup> , Gavriel Olshansky<sup>7,8</sup>, Alexander Dobrovic<sup>9</sup>, Anthony T. Papenfuss<sup>1,2,10,11,12</sup> and Terence P. Speed<sup>1,5,12</sup>

**Accurate identification and effective removal of unwanted variation is essential to derive meaningful biological results from RNA sequencing (RNA-seq) data, especially when the data come from large and complex studies. Using RNA-seq data from The Cancer Genome Atlas (TCGA), we examined several sources of unwanted variation and demonstrate here how these can significantly compromise various downstream analyses, including cancer subtype identification, association between gene expression and survival outcomes and gene co-expression analysis. We propose a strategy, called pseudo-replicates of pseudo-samples (PRPS), for deploying our recently developed normalization method, called removing unwanted variation III (RUV-III), to remove the variation caused by library size, tumor purity and batch effects in TCGA RNA-seq data. We illustrate the value of our approach by comparing it to the standard TCGA normalizations on several TCGA RNA-seq datasets. RUV-III with PRPS can be used to integrate and normalize other large transcriptomic datasets coming from multiple laboratories or platforms.**

**A**n essential step of RNA sequencing (RNA-seq) data analysis is normalization, whereby different sources of unwanted variation are removed to make gene expression measurements comparable within and between samples<sup>1–4</sup>. In cancer RNA-seq data, within-sample normalization should adjust for gene length, GC content and cellular compositions, whereas between-sample normalization should remove the impact of library size, tumor purity and batch effects on the data. Efficient removal of such variation from RNA-seq data is still a challenge. This variation can introduce artificial or obscure true biological signals in the data and, consequently, lead to false or missed discoveries, resulting in misleading biological conclusions<sup>1,5–8</sup>.

Most RNA-seq normalizations adjust for library size variation using global scaling factors calculated based on either total counts or other statistical features of the raw count data, such as their upper quartiles<sup>3,9,10</sup>. These normalizations simply divide all gene counts in each sample by a single scale factor. The implicit assumption underlying such methods is that all the gene-level counts are proportional to the scale factors and that it should be adequate to adjust them for library size in this way across samples. A current challenge for RNA-seq normalizations arises when the counts for a reasonable proportion of genes cannot be properly adjusted for library size by the use of a single scale factor, regardless of how it is computed. The bias between gene-level counts and library size has been discussed in single-cell RNA sequencing data<sup>11,12</sup>, however, this has not been recognized in RNA-seq data.

Tumor purity—that is, the proportion of cancer cells in solid tumor tissues—is another major source of variation in cancer RNA-seq data. This variation has been viewed as an intrinsic characteristic of tumor samples and has been linked to several clinical outcomes in patients with various cancer types<sup>13–16</sup>. Tumor purity could be considered as a source of unwanted variation in studies whose aims are restricted to tumor-specific expression. Variation in tumor purity can affect comparisons of a gene's expression within and between samples, which can compromise downstream analyses in cancer RNA-seq studies<sup>17–19</sup>. Current RNA-seq normalizations and batch correction methods are unable to remove this kind of variation from the data. Adjusting counts for tumor purity variation using regression models risks removing biological signal if that signal is confounded with purity.

Batch effects are obvious sources of unwanted variation in large RNA-seq studies, where samples are necessarily processed across a range of conditions—for example, chemistry, protocol and facility. Most batch correction methods are based on linear regression. For individual gene expression, they fit a linear model with blocking terms for batch. Then, the coefficient for each blocking term is set to zero, and the corrected expression values are computed from the residuals<sup>20–22</sup>. An implicit assumption underlying such methods is that the biological populations are evenly distributed within each batch—that is, that there is no association between batch and biological condition. However, if there is such an association (due to confounding), then correcting gene expression counts for batch

<sup>1</sup>Walter and Eliza Hall Institute of Medical Research, Parkville, Victoria, Australia. <sup>2</sup>Department of Medical Biology, The University of Melbourne, Melbourne, Victoria, Australia. <sup>3</sup>Biomedicine Discovery Institute and the Department of Biochemistry and Molecular Biology, Monash University, Clayton, Victoria, Australia. <sup>4</sup>Department of Statistics, University of Michigan, Ann Arbor, Ann Arbor, MI, USA. <sup>5</sup>School of Mathematics and Statistics, The University of Melbourne, Melbourne, Victoria, Australia. <sup>6</sup>Department of Economics and Statistics, Monash University, Melbourne, Victoria, Australia. <sup>7</sup>Metabolomics Laboratory, Baker Heart and Diabetes Institute, Melbourne, Victoria, Australia. <sup>8</sup>Baker Department of Cardiometabolic Health, The University of Melbourne, Melbourne, Victoria, Australia. <sup>9</sup>Department of Surgery, The University of Melbourne, Austin Health, Heidelberg, Victoria, Australia. <sup>10</sup>Peter MacCallum Cancer Centre, Melbourne, VIC, Australia. <sup>11</sup>Sir Peter MacCallum Department of Oncology, The University of Melbourne, Melbourne, Victoria, Australia. <sup>12</sup>These authors contributed equally: Anthony T. Papenfuss, Terence P. Speed. e-mail: [molania.r@wehi.edu.au](mailto:molania.r@wehi.edu.au); [papenfuss@wehi.edu.au](mailto:papenfuss@wehi.edu.au); [terry@wehi.edu.au](mailto:terry@wehi.edu.au)

effects using these methods risks removing biological signal along with the batch effects. Furthermore, batch effects usually influence subsets of genes in different ways<sup>6,8</sup>; sample-wise normalization, including normalizations that rely on global scaling factors, generally fail to remove this variation from the data.

We previously developed a normalization method, called removing unwanted variation III (RUV-III), for gene expression studies with technical replicates<sup>8</sup>. The RUV-III method is a linear model through which the presence and impact of known and unknown unwanted factors can be inferred via technical replicates and negative control genes. However, RUV-III has two limitations. First, it is not designed to be used effectively in situations where technical replicates are not available or well-distributed across the sources of unwanted variation. Second, because a sample's tumor purity will be essentially the same across all of its technical replicates, the original RUV-III is unable to estimate and remove this kind of variation using standard technical replicates.

Here we propose an approach, called pseudo-replicates of pseudo-samples (PRPS), to deploy RUV-III to efficiently remove the impact of library size, tumor purity and batch effects from RNA-seq data. The PRPS approach overcomes the limitations of RUV-III in situations where suitable technical replicates are not available or where variation due to tumor purity is to be removed from cancer RNA-seq data. To use RUV-III with PRPS, we first need to identify the sources of unwanted variation and major expression-based biological populations in the data. We then create pseudo-samples, which are *in silico* samples derived from small groups of samples that are roughly homogeneous with respect to unwanted variation and biology. Two or more pseudo-samples with the same biology will be regarded as a pseudo-replicate set. The gene expression differences between such pseudo-samples will largely be unwanted variation. RUV-III makes use of such differences, together with negative control genes, to estimate and remove unwanted variation from the data.

We make use of three RNA-seq datasets from The Cancer Genome Atlas (TCGA) studies to show that RUV-III with PRPS can effectively remove library size, tumor purity and batch effects and lead to meaningful biological results that are not compromised by this kind of variation. We will demonstrate that RUV-III with PRPS can be used to normalize multiple RNA-seq studies. We also present comprehensive strategies for revealing unwanted variation in large-scale RNA-seq studies, such as those of the TCGA project.

## Results

**TCGA RNA-seq datasets.** The TCGA Research Network generated RNA-seq data from ~11,000 tumor and normal sample tissues obtained from 33 cancer types. To understand some potential sources of unwanted variation, fresh-frozen tissue samples were collected from tissue source sites (TSSs), allocated to 96-well sequencing plates (hereafter called plates) and processed at various times

(Supplementary Table 1). Some TCGA RNA-seq datasets, such as uveal melanoma and kidney chromophobe, were generated using a single plate. In general, plates are completely confounded with times, making it difficult to distinguish plate effects from time effects. There are also formalin-fixed, paraffin-embedded samples among the TCGA RNA-seq samples, and these were excluded from the data discussed here. Low-quality samples and lowly expressed genes were also excluded from individual datasets before the analyses in this paper (Methods). The TCGA RNA-seq datasets are available in the form of raw gene counts, fragments per kilobase of transcript per million mapped reads (FPKM) and FPKM followed by upper-quartile normalization (FPKM.UQ).

**Library size, tumor purity and plate effects are major sources of unwanted variation across TCGA RNA-seq datasets.** We first considered the role of sample RNA-seq library size as a source of unwanted variation. Ideally, the gene-level counts should have no significant association with library size variation in a well-normalized dataset (Fig. 1a). Consequently, any downstream analysis, including dimensional reduction, gene co-expression and differential expression, should also not be influenced by library size variation.

For most TCGA RNA-seq studies, library sizes vary greatly both within and between years (Fig. 1b). The first five principal components (PC) cumulatively are strongly associated with (log) library size in the raw gene counts (Fig. 1c, first panel). The FPKM and FPKM.UQ normalizations reduced the effects of library size, but they showed shortcomings—high correlation between PCs and library size—in several cancer types (Fig. 1c, first panel). For each cancer type, the association between individual gene-level counts and library size was quantified using Spearman correlation (Fig. 1d, first panel, and Supplementary Fig. 2a). The results show that a large proportion of genes have high positive correlations with library size in the raw gene count datasets. However, in these datasets, there are reasonable numbers of genes whose expression levels have no correlation or a negative correlation with library size (Fig. 1d, first panel) and, thus, present a challenge for the standard RNA-seq normalizations. Supplementary Fig. 1 shows that the association between gene-level raw counts and library size is partially explained by average gene expression level and is never constant. The FPKM and FPKM.UQ normalizations introduce or exacerbate library size effects in genes whose expression has no or negative association with this variation. This will be discussed in more detail for the rectum adenocarcinoma (READ) and colon adenocarcinoma (COAD) RNA-seq datasets.

Next, we used linear regression and Spearman correlation analyses to quantify the variation in tumor purity in the TCGA RNA-seq datasets (Fig. 1c, second panel, and Fig. 1d, second panel). The results indicate the presence of substantial variation in tumor purity, and FPKM and FPKM.UQ normalizations cannot correct for this in the datasets (Fig. 1c, second panel, and Supplementary Fig. 2b). We discuss how the tumor purity variation can compromise

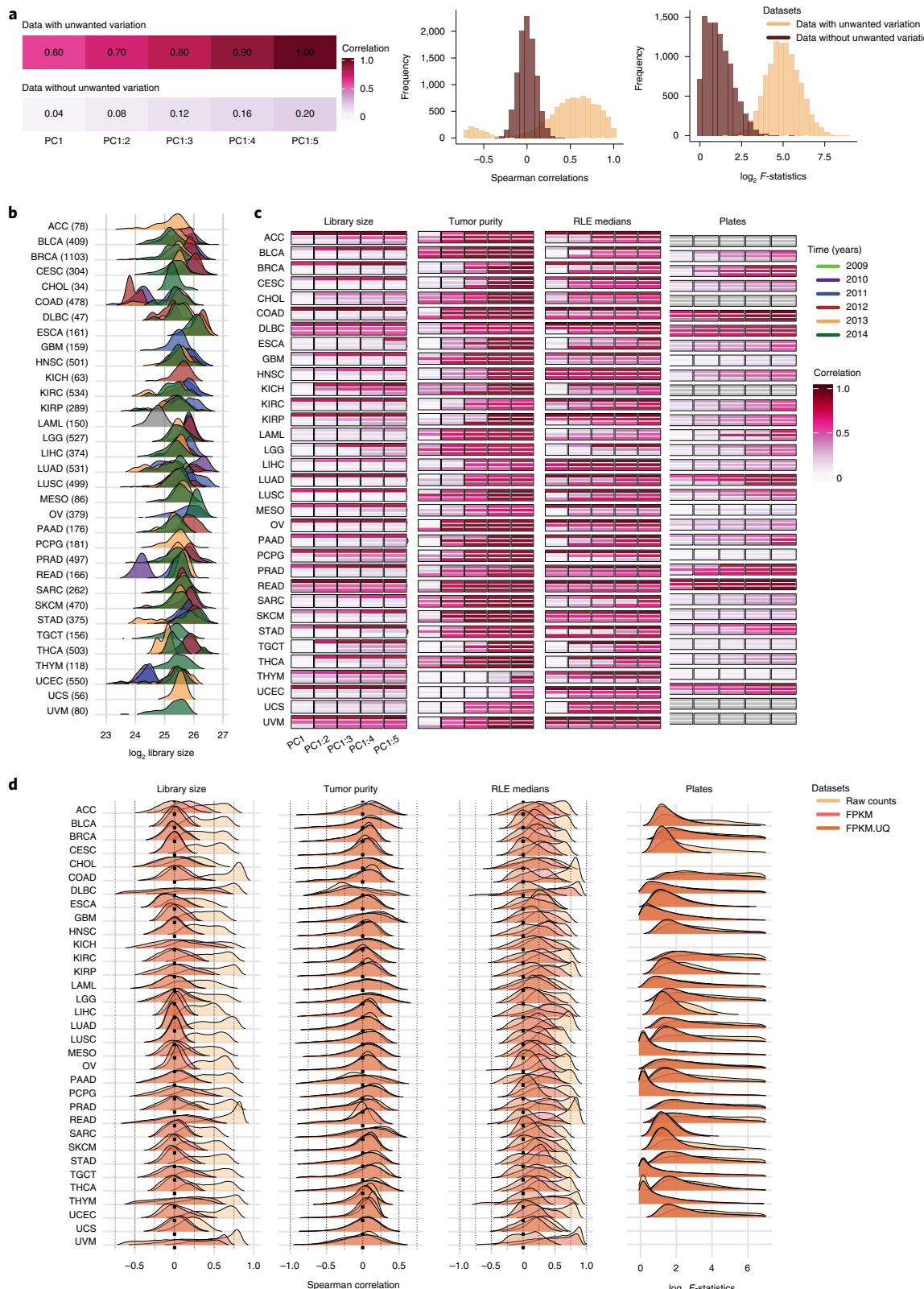
**Fig. 1 | Unwanted variation in individual TCGA RNA-seq datasets.** **a**, Illustrative examples showing data with and without unwanted variation. Data with unwanted variation exhibit high correlation between the first five PCs and this variation (top left). Data without unwanted variation have low correlation with unwanted variation (bottom left). The histograms show Spearman correlations and  $\log_2 F$ -statistics between individual genes and different sources of unwanted variation. Data with large library size and tumor purity variation show high Spearman correlations between individual gene expression and this variation. Data with plate effects exhibit high  $F$ -statistics obtained from ANOVA between individual gene expression and plates as factor. In contrast, data without such unwanted variation show low Spearman correlations and  $F$ -statistics. **b**, Distribution of ( $\log_2$ ) library size colored by years for the individual TCGA cancer types. The year information was not available for the LAML RNA-seq study. The library sizes are calculated after removing lowly expressed genes for each cancer type. **c**,  $R^2$  obtained from linear regression between the first, first and second, and so on, cumulatively to the fifth PC and library size (first panel), tumor purity (second panel) and RLE medians (third panel) in the raw count, FPKM and FPKM.UQ normalized datasets. The fourth panel shows the vector correlation between the first five PCs cumulatively and plates in the datasets. Ideally, we should see no significant associations between PCs and sources of unwanted variation. Gray color indicates that samples were profiled across a single plate. **d**, Spearman correlation coefficients between individual gene expression levels and library size (first panel), tumor purity (second panel) and the RLE medians (third panel) in the datasets. The fourth panel shows  $\log_2 F$ -statistics obtained from ANOVA of gene expression levels by the factor: plate variable. Plates with fewer than three samples were excluded from the analyses. ANOVA was not possible for cancer types whose samples were profiled using a single plate.

downstream analyses, including gene co-expression and subtype identification, as was observed in the TCGA breast invasive carcinoma (BRCA) RNA-seq data.

In most TCGA RNA-seq studies, biospecimens were profiled necessarily across plates, which can impact on gene expression levels. Vector correlation and analysis of variance (ANOVA) (Methods) reveal the presence of plate effects in the raw gene counts, FPKM

and FPKM.UQ normalized datasets (Fig. 1c, third panel). We found that the major known biological populations are well-distributed across plates in TCGA READ, COAD, lung adenocarcinoma and BRCA RNA-seq data, showing the absence of large confounding effects in the data.

Finally, we examined the medians of relative log expression (RLE)<sup>23</sup> for the raw count and TCGA normalized datasets



(Methods). In the absence of unwanted variation, the RLE medians should be centered around zero, so any deviation from zero indicates the presence of unwanted variation in the data. Supplementary Fig. 3 illustrates that the RLE medians of the raw count datasets deviate greatly from zero, which further confirms the presence of unwanted variation. We then investigated the associations between the first five PCs cumulatively and the RLE medians (Fig. 1c, third panel) and also computed the Spearman correlation between individual gene expression with the RLE medians for each cancer type (Fig. 1d, third panel). Ideally, we should see no associations; however, we see many associations in the raw counts and the FPKM and FPKM.UQ normalized datasets. We will demonstrate the importance of scrutinizing the association between the RLE medians and both principal component analysis (PCA) and individual gene expression in the TCGA breast cancer RNA-seq data.

Taken together, our results show that all the TCGA RNA-seq datasets, both raw and normalized, are greatly affected by the three major sources of unwanted variation. Next, we used the READ, COAD and BRCA RNA-seq datasets to illustrate the effects of unwanted variation on certain downstream analyses and show the performance and effectiveness of RUV-III with PRPS for these datasets. The details of each study are provided separately below.

**TCGA READ RNA-seq study. Study outline.** The READ RNA-seq study involved 176 assays generated using 14 plates over 4 years. The RNA-seq library sizes vary greatly between samples profiled in 2010 and the other samples (Supplementary Fig. 4). The major gene-expression-based biological populations—consensus molecular subtypes (CMSs)<sup>24</sup>—were identified using the R package CMScaller<sup>25</sup> (Methods) in the data normalized by different methods. See Supplementary Figs. 5 and 6 and the Supplementary File for further details. These subtypes will be used for both assessing the performance of normalization methods and creating PRPS for RUV-III normalization.

**RUV-III removes substantial library size variation and plate effects from the data.** Substantial library size variation between samples profiled in 2010 and the other samples are clearly visible in the RLE and PCA plots (Supplementary Fig. 7a and Fig. 2a, top panel) of the raw count data. Although the FPKM and FPKM.UQ normalizations reduced this variation, both methods exhibited shortcomings—for example, by not fully mixing samples with large library size differences (Fig. 2a, top row).

PCA plots and linear regression between the first five PCs cumulatively and library size clearly illustrate that RUV-III with PRPS improved upon the FPKM and FPKM.UQ normalizations in removing the variation in library size from the data (Fig. 2a, top row, and Fig. 2b, top plot).

Spearman correlation analyses between the individual gene expression values and library size reveal a large proportion of genes showing strong positive or negative correlations with library size in the FPKM and FPKM.UQ normalized datasets, whereas this correlation was significantly reduced in the RUV-III normalized data (Fig. 2b, bottom). Furthermore, differential expression (DE) analysis (Methods) was performed between samples with high and low library size. Ideally, we should see little evidence of differential gene expression, whereas we see a lot in the FPKM and FPKM.UQ datasets, far more than in the RUV-III normalized data (Fig. 2c, top). Finally, the silhouette coefficient and adjusted Rand index (ARI) analyses (Methods) showed that RUV-III performs better in mixing the samples with large library size differences (Fig. 2c, bottom).

To examine plate effects and separate this variation from the large library size variation in the data, we performed our evaluation within each key time interval. The results showed that RUV-III clearly improves over the FPKM and FPKM.UQ normalizations in removing plate effects from the data (Fig. 2d).

Note that, here we have not attempted to remove variation caused by tumor purity. Consequently, the tumor purity estimates obtained from the RUV-III and FPKM.UQ normalized data were highly correlated (Supplementary Fig. 7b). This illustrates the ability of RUV-III to remove only the variation that the user wants to remove and no more—that is, to retain other variation that is of biological origin.

We next explored the relationship between RLE medians and both library size and tumor purity—the two major variations in the data—for the different normalizations (Supplementary Fig. 7c). The library size variation is the largest variation in the raw counts data, and RLE medians are strongly associated with this variation. The TCGA and RUV-III normalizations reduced the variation in the library size; therefore, the tumor purity became the largest variation in these datasets. Then, the RLE medians of the TCGA and RUV-III normalized data show a strong association with tumor purity (Supplementary Fig. 7d). These results were further supported by comparisons of the Spearman correlation analyses between the individual gene expression levels and RLE medians with the same analyses between the individual gene expression levels and library size and with tumor purity (Supplementary Fig. 8). Together, these results show the value of exploring the association of the RLE medians with known sources of unwanted variation in the data. Later, we will show that the RLE medians have no correlation with gene expression in the TCGA BRCA RUV-III normalized data when variations in both library size and tumor purity are removed.

**RUV-III improves the separation between consensus molecular subtypes.** Colorectal cancers are classified into four transcriptomic-based subtypes—CMSs—with distinct features<sup>24</sup>. PCA plots of the RUV-III normalized data show distinct clusters of the CMSs for the READ RNA-seq samples, whereas these subtypes are not as clearly separated in the TCGA normalized datasets (Fig. 2a, bottom row). To confirm the pattern of the CMS clusters in the PCA plots of the RUV-III normalized data, we applied PCA within the key time intervals in the FPKM and FPKM.UQ normalized datasets. The results show that the CMS clustering within each time interval in the FPKM.UQ data is highly consistent with that obtained with RUV-III using the full set of data (Supplementary Fig. 9).

Furthermore, the vector correlation analysis between the first five PCs cumulatively and the CMS confirmed that the RUV-III normalization leads to a better separation of the CMS clusters than the TCGA normalized datasets (Fig. 2e, top). These results were strengthened by silhouette coefficient and ARI analyses (Fig. 2e, bottom). Additionally, gene set enrichment analyses showed that the CMSs obtained from the RUV-III normalized data are associated with known gene signatures<sup>25</sup> (Supplementary Fig. 6b). Supplementary Fig. 10 shows the Kaplan–Meier survival plots of the CMSs identified by different normalization methods. The survival outcome difference between CMS2 and CMS4 that were obtained from the RUV-III normalized data is clearer than the TCGA normalized datasets (Supplementary Fig. 10).

**RUV-III improves gene co-expression and gene-level survival analyses.** Unwanted variation introduced by the large sample library size differences can compromise downstream analyses, such as gene co-expression and gene-level survival analyses, in the TCGA READ RNA-seq data. This variation can have two effects on gene co-expression analysis. It can lead to apparent correlations between genes that are most likely un-correlated. For example, the correlation between the *TMF1* (TATA element modulatory factor 1) and *BCLAF1* (Bcl-2-associated transcription factor 1) genes are  $p=0.8$  and  $p=0.7$  in the TCGA FPKM and FPKM.UQ normalized data, respectively. The role of the *TMF1* gene has not been characterized in COAD, although the *BCLAF1* gene shows a pro-tumorigenic role in this cancer type<sup>26</sup>. One might suggest that the *TMF1* gene expression

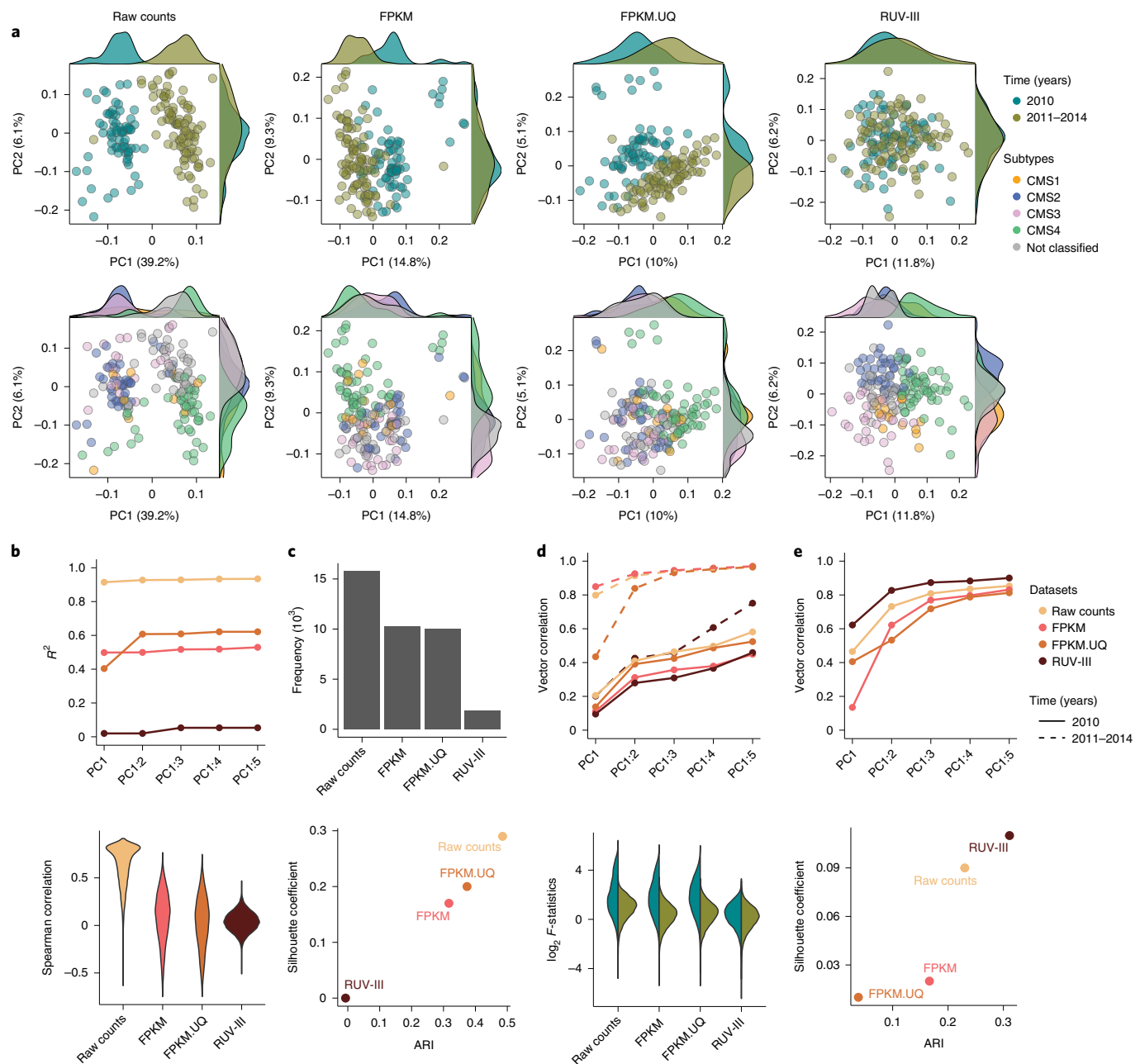


**Fig. 2 | Performance assessment of different normalizations on the TCGA READ RNA-seq data.** **a**, Top row: scatter plots of first two PCs for raw counts, FPKM, FPKM.UQ and RUV-III normalized data colored by key time intervals (2010 versus 2011–2014). Bottom row: same as the top row colored by the CMS. The CMSs were obtained for each dataset separately. **b**, Top: a plot showing the  $R^2$  of linear regression between library size and up to the first five PCs (taken cumulatively). Bottom: violin plots of Spearman correlation coefficients between the gene expression levels and library size for individual data. **c**, Top: the frequency of  $P < 0.05$  obtained from DE analysis between samples with low and high library size. Bottom: Scatter plot shows silhouette coefficients and ARI for mixing samples from two different key time intervals. **d**, Top: a plot showing the vector correlation coefficient between plates and the first five PCs within each time intervals. Bottom: box plots of  $\log_2 F$ -statistics obtained from ANOVA within each key time interval for gene expression with plate as a factor. **e**, Top: a plot showing the vector correlation coefficient between CMS subtypes and up to the first five PCs. Bottom: a scatter plot displays silhouette coefficients and ARI for measuring the separation of CMS subtypes.

may have a role in tumorigenesis in colon cancer due to its high correlation with the *BCLAF1* gene expression. However, we see no such correlation in the RUV-III normalized data, which is consistent with the correlation obtained from an independent platform, namely the TCGA READ microarray data (Fig. 3a). On the other hand, the unwanted variation can obscure correlations between gene–gene expression levels that are likely to be truly correlated. For example, the overall correlation between the *MDH2* (malate dehydrogenase 2)

and *EIF4H* (eukaryotic translation initiation factor 4H) genes is  $\rho = -0.05$ , whereas they exhibit a high correlation within each key time interval in the TCGA normalized data (Fig. 3a). The overall correlation of these genes was 0.7 in the RUV-III normalized data, consistent with what was seen in the TCGA READ microarray data (Fig. 3a). The *MDH2* and *EIF4H* genes show important roles in cancer growth and metastasis; thus, they are of clinical importance for cancer treatment<sup>27,28</sup>. The high correlation between these two

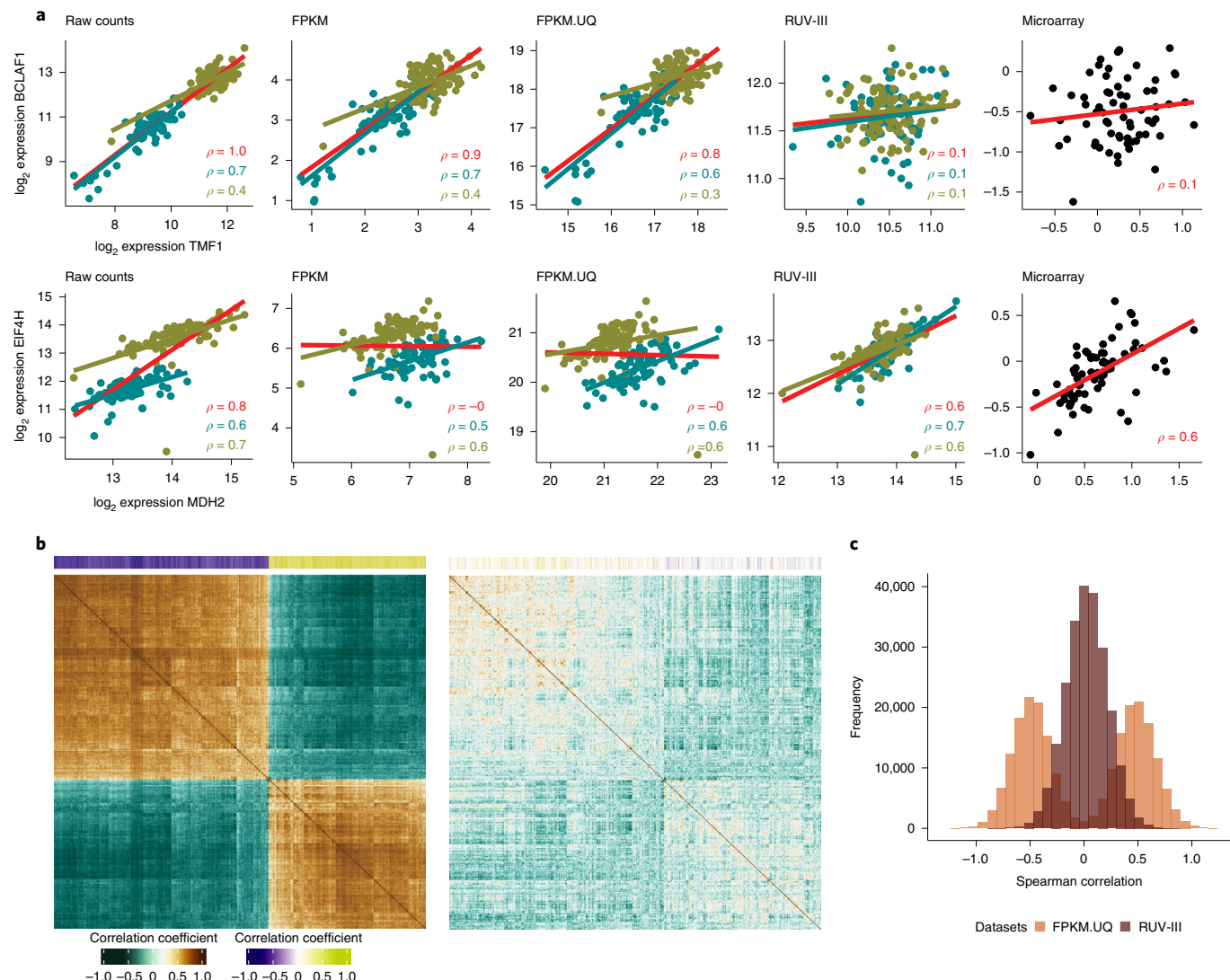


**Fig. 3 | Gene co-expression analyses of TCGA READ RNA-seq data using different normalizations.** **a**, First row: scatter plots of the gene expression levels of the *TMF1* and *BCLAF1* genes in the TCGA READ raw counts and differently normalized datasets. The red line shows overall association, and the cyan and olive lines show associations between the gene expression within 2010 samples and within the rest of the samples, respectively. Second row: same as the first row, for *MDH2* and *EIF4H* gene expression. **b**, The correlation matrix of expression levels of the genes with the 500 highest correlations with library size in the FPKM.UQ. The first plot is obtained using FPKM.UQ, and the second plot is obtained using the RUV-III normalized data. The colored bar along the top shows the correlation of individual genes with library size. The order of rows and columns is the same in both correlation matrices. **c**, Differences ( $\rho_{\text{microarray}} - \rho_{\text{RNA-seq}}$ ) of Spearman correlation coefficients for all possible gene-gene pairs calculated using the TCGA READ microarray and both the FPKM.UQ and RUV-III normalized RNA-seq data.

genes revealed by RUV-III may suggest that they are involved in a co-expression network, which has not been previously reported.

We extended this analysis to all possible gene–gene correlations of the genes that have the highest correlation with library size in the FPKM.UQ normalized data (Fig. 3b). Strikingly, the results show numerous strong but likely spurious correlations between gene pairs in the FPKM.UQ normalized data, whereas using RUV-III significantly reduced these correlations (Fig. 3b).

Figure 3c depicts the differences ( $\rho_{\text{microarray}} - \rho_{\text{RNA-seq}}$ ) between all possible gene–gene Spearman correlation coefficients  $\rho$  using the TCGA READ microarray data and the FPKM.UQ and RUV-III normalized data.

Association between gene expression and survival outcomes of patients is another downstream analysis that can be influenced by the library size variation in the TCGA READ RNA-seq data. For example, RUV-III, as opposed to the TCGA normalized data, revealed that the expression of the *RAB18* (Ras-related in

18) and *FBX14* (F-box and leucine-rich repeat protein 14) genes are highly associated with overall survival outcome of patients in the data (Fig. 4). The reason is clear from the expression patterns across time: dividing samples based on median expression mainly resulted in two groups with low and high library size, which was not biologically meaningful for the TCGA normalizations (Fig. 4). *RAB18* gene expression plays pivotal roles in cell proliferation and metastasis, and high expression is associated with poor survival in different cancer types<sup>29</sup>. *FBX14* gene expression mediates the epithelial–mesenchymal transition (EMT) in cancer, which indicates that *FBX14* could function as an EMT inhibitor to suppress metastasis in human cancers<sup>30</sup>. Other examples are *PTPN14* and *CSGALNACT2*, whose associations with survival have been previously shown in colorectal cancer (Supplementary Fig. 11)<sup>31</sup>. We found a remarkable number of genes whose expression levels were associated with survival using the RUV-III

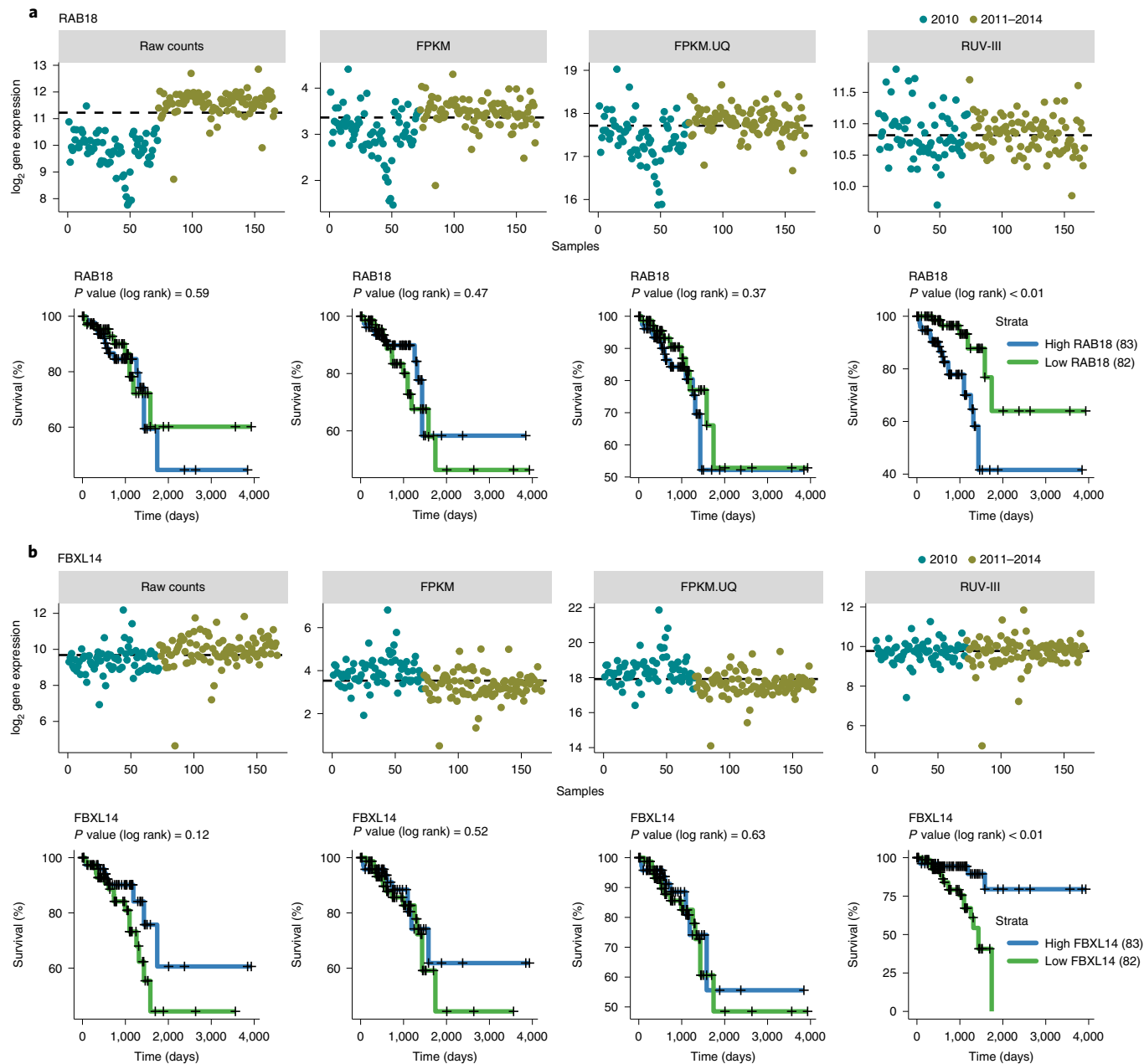


**Fig. 4 | Association between gene expression and overall survival in differently normalized TCGA READ datasets. a.** Upper part: plots of the expression levels of the *RAB18* gene across samples. The dashed lines represent the median expression level of the *RAB18* gene. Lower part: Kaplan-Meier curves for samples with low (below median) and high (above median) expression of the *RAB18* gene. **b.** As in **a** for the *FBXL14* gene.

normalized data, which were not found using the FPKM and FPKM.UQ normalized data.

*Gene-level counts are not proportional to library size.* The FPKM and FPKM.UQ normalizations rely on global scale factors computed based on library size or upper quartiles of samples in the raw count data (Fig. 5a) to remove library size effects. These methods assume that gene-level counts all are proportional to the global scale factors. However, we show that, in the READ raw count data, different groups of genes exhibit different relationships to the global scale factors used in the FPKM and FPKM.UQ normalizations (Fig. 5b).

The first group consists of genes whose counts are proportional to the global scale factors. For these genes, the FPKM and FPKM.UQ normalizations are adequate to remove the association between

library size variation and gene expression. The *DDX23* (DEAD-box helicase 23) gene is an example from this group (Fig. 5c, first row). The second group includes genes whose expression levels are greater than those expected using the global scaling factors, and so those factors are insufficient for adjusting their expression levels to be independent of library size. The *LARP7* (La ribonucleoprotein 7) gene represents the behavior of genes in this group (Fig. 5c, second row). The third group contains genes such as *ALKBH7* (AlkB homolog 7), whose expression levels are not associated with library size in the raw count data. Then, the FPKM and FPKM.UQ normalizations introduce the library size variation to the expression levels of genes in this group (Fig. 5c, third row). Finally, there are genes such as *TMEM160* (transmembrane protein 160) whose expression levels relate to library size in a manner opposite to that motivating

the use of global scaling factors. Applying scaling factors to such genes exacerbates, rather than removes, variation associated with library size (Fig. 5c, fourth row).

Note that we found the same issue in the TCGA RNA-seq datasets, such as kidney chromophobe and uveal melanoma, where samples were profiled using a single plate (Fig. 1c, first panel, and Supplementary Fig. 12).

**TCGA COAD RNA-seq study.** The COAD RNA-seq study involved 479 assays generated across 4 years. As with the READ RNA-seq data, there are large library size differences between samples profiled in 2010 and the other samples. The FPKM and FPKM.UQ normalizations removed library size effects from the data more effectively than was the case for the READ RNA-seq data, but these also had shortcomings.

It should be noted that the first two PCs of the FPKM and FPKM.UQ data did not reveal that the library size effects have not been properly removed. This highlights the importance of gene-level assessment, such as correlation between individual gene expression and library size or DE analysis between batches, to assess the performance of normalizations. See the Supplementary File and Supplementary Figs. 13–25 for full details of this dataset and results analogous to those just presented for the READ data.

**TCGA BRCA RNA-seq study. Study outline.** The BRCA RNA-seq study involved 1,180 assays that were carried out on samples from 40 TSSs, distributed across 38 plates, and profiled over 5 years from 2010 to 2014 (Supplementary Fig. 26). The samples collected in 2010 and 2011 were profiled using one flow cell chemistry, and the remaining samples were profiled using a different flow cell chemistry (personal communication from TCGA). There were 94 adjacent normal breast tissue samples and seven paired primary-metastatic samples in the study (Supplementary Fig. 26). The major intrinsic biological populations, prediction analysis of microarray 50 (PAM50) of the TCGA BRCA RNA-seq samples, were identified using different approaches. See the Supplementary File and Supplementary Figs. 27 and 28 for full details.

**RUV-III removes the effects of tumor purity, flow cell chemistries and library size.** As with most of the other TCGA RNA-seq studies (Fig. 1), tumor purity is one of the major sources of variation in the BRCA study. For this dataset, we designed our PRPS to remove the effects of tumor purity as well as other technical variation (Methods).

Linear regression between the first five PCs cumulatively and tumor purity within the individual PAM50 subtypes showed that the RUV-III normalization substantially removed this variation from the data (Fig. 6a). These results were supported by Spearman correlation analyses between individual gene expression levels and tumor purity within each of the PAM50 subtypes and a DE analysis between samples with low and high tumor purity (Fig. 6b,c). The variation of tumor purity estimated using the RUV-III normalized data was significantly smaller than that observed in the corresponding measurements on the FPKM.UQ normalized data (Fig. 6d).

As mentioned above, the TCGA BRCA RNA-seq samples were profiled over two batches of flow cell chemistries. PCA plots of the FPKM and FPKM.UQ normalized datasets showed noticeable variation due to the use of two flow cell chemistries, whereas RUV-III effectively removed this variation from the data (Supplementary Fig. 29a). This conclusion was supported by a vector correlation

analysis between the first ten PCs cumulatively and the binary flow cell chemistry variable, silhouette analyses, the ARI and ANOVA between individual gene expression measurements and the flow cell chemistry factor (Fig. 6e–g and Supplementary Fig. 29b,c).

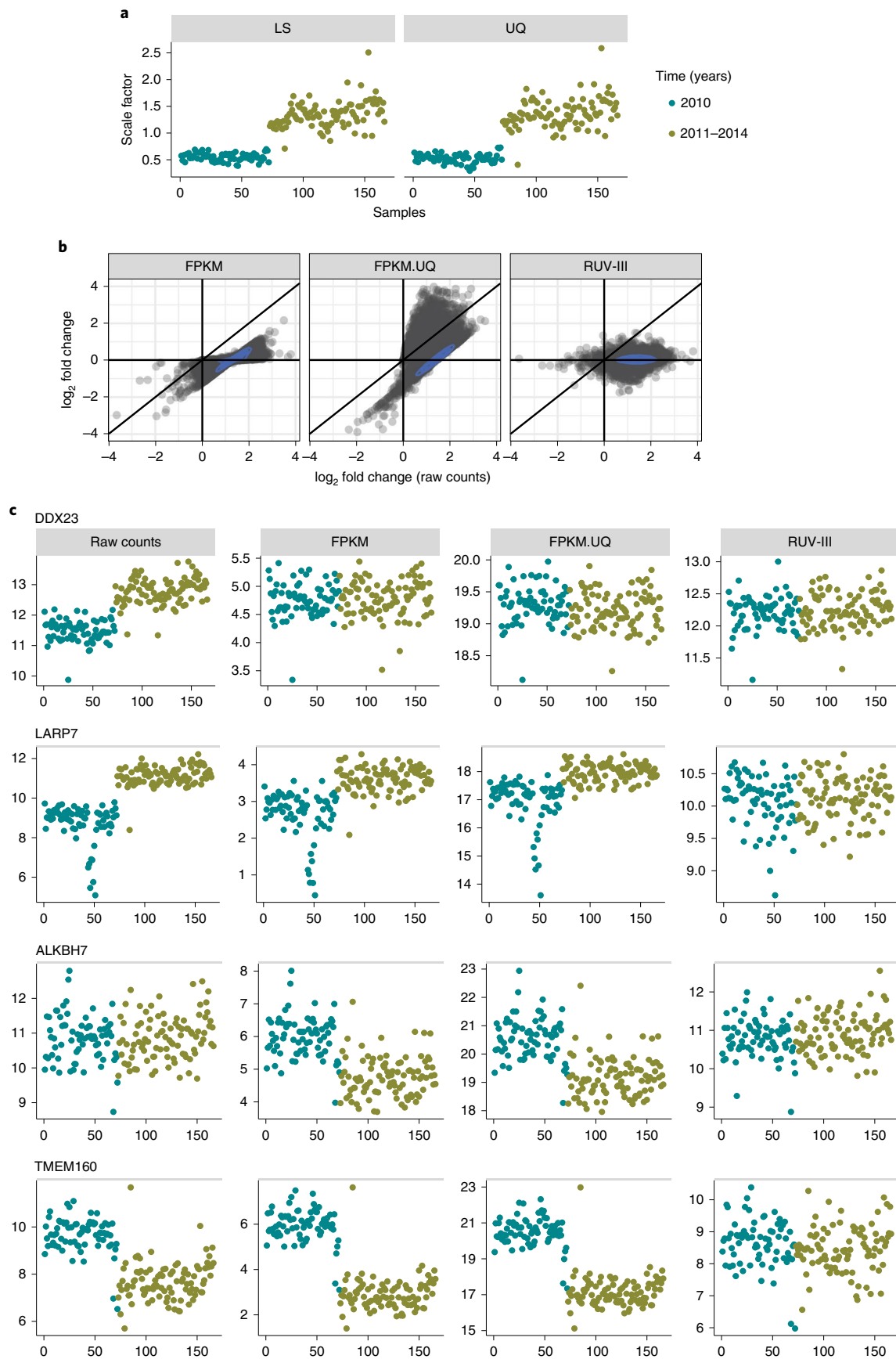
An expression heat map of the most highly affected genes by the flow cell chemistries showed that different genes are affected in different ways (Fig. 6h). Interestingly, the heat map also revealed two clusters within the samples processed by the first flow cell chemistry. This suggests that there are additional sources of unwanted variation of unknown origin within each flow cell chemistry. To explore this more fully, we took the set of most highly affected genes by the flow cell chemistries and scored samples against this gene set (hereafter called the batch score) using the R/Bioconductor package *singscore*<sup>32</sup> on the FPKM.UQ normalized dataset. Batch scores clearly distinguished samples from the flow cell chemistry batches and separated the samples into clusters within each flow cell chemistry (Fig. 6i). We then used cutoffs to divide the samples into four groups based on their batch scores. These groups were not visible in the batch scores obtained from the RUV-III normalized data (Fig. 6i). Spearman correlation analyses showed that a surprising number of genes had either high positive or high negative correlations with the batch scores in the FPKM.UQ normalized data (Fig. 6j), whereas these correlations were much lower in the RUV-III normalized data.

**Tumor purity and flow cell chemistries effects compromise gene co-expression and survival analysis.** Just as we saw above with library size, tumor purity variation can affect downstream analyses, such as gene co-expression and the association between gene expression levels and survival outcomes of patients in the data. As with library size, this variation can introduce correlation between genes that are probably un-correlated. For example, Fig. 7a shows that the gene expression levels of *ZEB2* (zinc finger E-box-binding homeobox 2) and *ETS1* are both highly correlated with tumor purity. The *ZEB2* gene is a one of the regulators of the EMT process that induces invasion of cancer cells<sup>33,34</sup>. *ETS1* is member of a large family of transcription factors characterized by their ETS DNA-binding domain. The gene appears to have dichotomous roles as an oncogene and a tumor suppressor gene in different cancer types<sup>35,36</sup>. The high correlation of *ETS1* with *ZEB2* in the TCGA BRCA RNA-seq data may confirm its oncogene role, but this is most likely a consequence of their correlations with tumor purity. The RUV-III normalized data and the breast cancer laser microdissection microarray data<sup>37</sup> showed that the expression levels of these two genes are uncorrelated (Fig. 7b).

To extend this observation, we selected 1,300 genes whose gene expression levels are highly correlated with tumor purity and then calculated Spearman correlations between all possible pairs of these genes. In a matching analysis, we computed partial correlations between these pairs adjusting for tumor purity (Methods). Figure 7c shows that there are many gene pairs that have high correlations, but these are mostly likely a consequence of their correlation with tumor purity.

Variation in tumor purity can also affect the association between gene expression levels and survival outcomes. For example, the expression of the *ZEB2* gene shows to be associated with cancer progression and survival outcome in different cancer types<sup>38,39</sup>. The RUV-III normalization revealed that high expression of the *ZEB2* gene is associated with a poor outcome in the TCGA BRCA RNA-seq data, but this was obscured by variation in tumor purity in the FPKM.UQ normalized data.

**Fig. 5 | Relationship between gene-level ( $\log_2$ ) counts and ( $\log_2$ ) library size in the TCGA READ RNA-seq data. a**, Global scale factors obtained by sample library sizes (LS) (left) and upper quartiles (UQ) (right) of READ raw counts versus time. **b**, Scatter plots of  $\log_2$  fold change obtained from DE analyses of gene expression levels with the major time variation: 2010 versus 2011–2014; ( $\log_2$ ) raw READ counts on the horizontal axes of all plots and differently normalized counts vertically. **c**, Expression patterns of four genes (*DDX23*, *LARP7*, *ALKBH7* and *TMEM160*) whose counts have different relationships with the global scaling factors calculated from the TCGA READ raw count data.



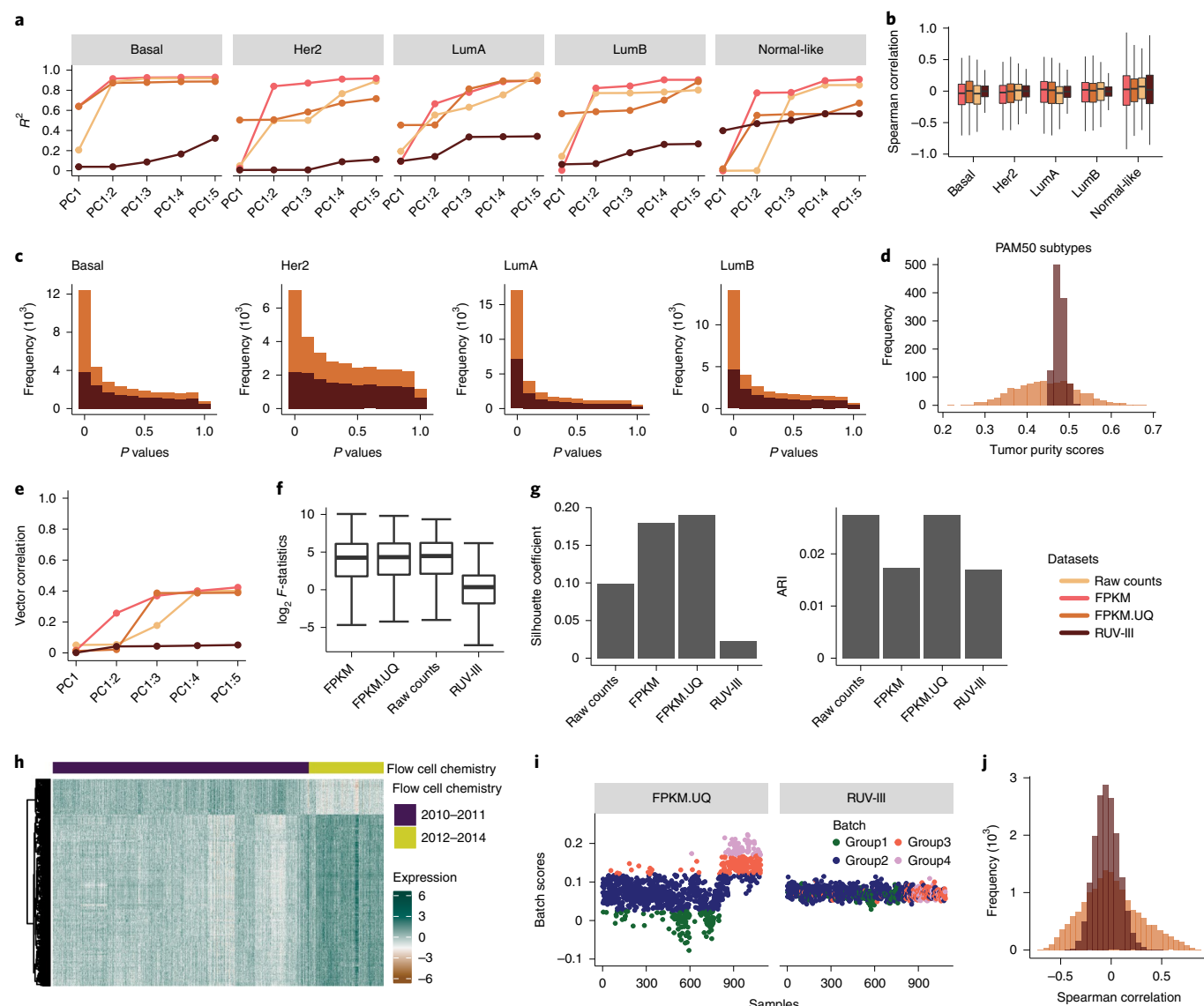


**Fig. 6 | RUV-III removes tumor purity and flow cell chemistry variation from the TCGA BRCA RNA-seq data.** **a**,  $R^2$  obtained from linear regression between the first five PCs (cumulatively) and tumor purity within individual PAM50 subtypes in the differently normalized datasets. The numbers of samples for each subtype and normalization are shown in Supplementary Fig. 27a. **b**, Box plots of Spearman correlation coefficients between individual gene expression and tumor purity levels in the differently normalized datasets ( $n=16,537$  genes). **c**, Unadjusted  $P$  value histograms of DE analysis between samples with low and high tumor purity within the four main PAM50 subtypes in the FPKM.UQ and the RUV-III normalized datasets.  $P$  values were obtained using Wilcoxon signed-rank test. **d**, Distributions of tumor purity scores in the FPKM.UQ and RUV-III normalized datasets. **e**, Vector correlation between the first five PCs (cumulatively) and flow cell chemistry in the normalized datasets. **f**, Box plots of  $\log_2 F$ -statistics obtained from ANOVA between individual gene expression levels and the flow cell chemistry factor in the differently normalized datasets ( $n=16,537$  genes). **g**, Bar charts of silhouette coefficients and ARIs showing the performance of different normalization methods in mixing samples from the two flow cell chemistries. **h**, Gene expression heat map of the 400 genes that are highly affected by the flow cell chemistries in the TCGA FPKM.UQ data (rows are clustered; columns are in chronological order of sample processing). **i**, Batch scores across samples in the FPKM.UQ (left) and RUV-III (right) normalized datasets. The batch scores were calculated by the singlScore method using the 400 genes described in **h**. Samples were divided into four groups based on their batch scores. **j**, Spearman correlation coefficients between the batch scores and individual gene expression levels in the FPKM and RUV-III normalized datasets. In the box plots (**b** and **f**), the heavy middle line represents the median; the box shows the IQR; the upper and lower whiskers extend from the hinges no further than  $1.5 \times$  IQR; and any outliers beyond the whiskers are shown as points.

Another example is the *STAB1* (stabilin 1) gene, whose expression levels are associated with survival in several cancer types, including breast cancer<sup>40–42</sup>. However, this association was only evident in the present data after removing variation in tumor purity. We found many more examples of such genes using the RUV-III normalized data.

The complex unwanted variation arising from the change in flow cell chemistry and the unknown source noted above clearly compromises estimates of gene co-expression in the FPKM.UQ normalized dataset. It introduces correlations between pairs of genes that are most likely not correlated. For example, the expression levels of the *ESRRA* (estrogen-related receptor alpha) and *MAP3K2*

(mitogen-activated protein kinase kinase kinase 2) genes are positively correlated in this dataset; however, this correlation seems to be a consequence of the unwanted variation in the data (Fig. 7e), for we do not see it in either the RUV-III normalized data or the TCGA BRCA microarray data (Fig. 7f).

To extend this analysis, we first selected the genes that had the 1,000 highest correlations with the batch scores in the FPKM.UQ normalized data and calculated all gene–gene correlations between them in both the FPKM.UQ and RUV-III normalized datasets. Figure 7j shows that a large number of gene pairs have high correlations in the FPKM.UQ normalized data, something we do not see in the RUV-III normalized data.

Interestingly, the overall correlation between expression of the *E2F4* (E2F transcription factor 4) and *CNOT1* (CCR4-NOT transcription complex subunit 1) genes is  $\rho=0.1$ , and the average of the correlations of these genes within each of groups 1–4 of the unknown source of unwanted variation is  $\rho=0.4$  (Fig. 7i) in the FPKM.UQ normalized data. Both the RUV-III normalized and the TCGA microarray data show a high positive correlation between the expression levels of the *E2F4* and *CNOT1* genes.

Supplementary Fig. 30 shows that the RUV-III normalization removed library size effects from this dataset more effectively than was the case with the FPKM and FPKM.UQ normalizations.

**RUV-III improves the separation of the PAM50 clusters.** Breast cancer intrinsic subtypes, including HER2-enriched, basal-like, luminal A, luminal B and normal-like<sup>43,44</sup>, are based on a 50-gene expression signature (PAM50)<sup>45</sup>. PCA plots, vector correlation between the first ten PCs cumulatively and the PAM50 subtypes, silhouette coefficients and ARI (Extended Data Fig. 1a–c) all show that the RUV-III normalization led to better separation of PAM50 subtypes in the BRCA RNA-seq data. Kaplan–Meier survival analysis shows that the PAM50 calls obtained using RUV-III normalized data exhibit significant associations with overall survival outcomes of TCGA BRCA patients (Supplementary Fig. 27b,c).

It should be noted the PAM50 subtypes identified using the TCGA normalized datasets are compromised by tumor purity, particularly samples from normal-like subtype that show very low tumor purity. We applied the PAM50 classifier on the breast cancer laser capture microdissection (LCM) gene expression data and found no normal-like subtype in the dataset. The results confirm previous studies that show that the normal-like subtype is due to the low tumor purity of samples<sup>46–48</sup>.

Additionally, Spearman correlation analysis showed that several of the PAM50 genes exhibit high correlation with tumor purity in the FPKM.UQ normalized data (Extended Data Fig. 1d). For example, expression of *FOXA1* (forkhead box A1) is highly associated with tumor purity in the Her2, luminal A and luminal B subtypes in the FPKM.UQ normalized data (Extended Data Fig. 1e). This observation suggests that variation in tumor purity might compromise the identification of PAM50 subtypes. In addition, this might also explain the differences between the PAM50 calls obtained from RUV-III normalized data, where the variation of tumor purity has been removed, and those obtained from the FPKM and FPKM.UQ normalized datasets (Supplementary Fig. 27a).

We explored the association between the expression levels of the PAM50 genes and survival within each of the PAM50 subtypes using both the FPKM.UQ and RUV-III normalized data. Interestingly, we found with the RUV-III normalized data that higher expression of the *FOXA1* gene is associated with poorer outcome in the luminal B subtype, a conclusion that was obscured by the variation in tumor purity of the TCGA RNA-seq data (Extended Data Fig. 1f).

**Normalization of multiple RNA-seq studies.** We assessed the performance of RUV-III with PRPS on the normalization of multiple RNA-seq studies. In this analysis, we normalized three large breast

cancer RNA-seq datasets, including TCGA and two cohorts from Brueffer et al. studies<sup>49,50</sup>. We did not have access to the raw counts data of Brueffer et al. studies, so we performed our normalization on the FPKM counts of all three studies. The lowly expressed genes were identified using the TCGA BRCA raw counts and removed from the other datasets. The PCA and RLE plots of the combined datasets show large variation between the TCGA and the other two studies (Supplementary Fig. 32a and 32b). As discussed above, we first need to identify sources of unwanted variation to create PRPS for RUV-III normalization. We used plates as batches for the TCGA BRCA RNA-seq data and the RLE medians (Methods) within each of the other two studies to identify batches. Their medians were clustered into three groups within each study. We performed PCA within each study using a set of RNA-seq house-keeping genes as negative control genes to explore the batches that were identified using the RLE medians. Supplementary Fig. 32c shows that the first and third PCs capture those batches. Then, the PAM50 subtypes were used as known major biological populations to produce five sets of PRPS (Supplementary Fig. 33a). The results demonstrated that RUV-III with PRPS leads to a satisfactory normalization by removing between-study and within-study variations and preserving the PAM50 clusters (Supplementary Fig. 33), whereas the other normalizations, quantile and upper quartile, show visible shortcomings. Furthermore, Supplementary Fig. 33d shows that several well-known gene–gene correlations<sup>51</sup> have been preserved in the RUV-III normalized data. We also explored the correlation between the two pairs of genes, *CNOT1\_E2F4* and *MAP3K2\_ESRRA*, that were discussed in the TCGA BRCA RNA-seq data (Fig. 7). The true correlation between these two pairs of genes was preserved in the RUV-III normalized data (Supplementary Fig. 33d). The results demonstrate that RUV-III with PRPS is applicable to normalizing RNA-seq data from multiple studies. Note that we would have preferred to use RUV-III on the raw counts without any further normalization, but we were unable to do so here.

**Performance of RUV-III with poorly chosen PRPS.** We evaluated the performance of RUV-III with poorly chosen PRPS on the TCGA READ and BRCA RNA-seq studies. To simulate poorly chosen PRPS, we randomly shuffled 20%, 40%, 60% and 80% of the biological labels, including the CMS and PAM50 subtypes, that were originally used to create PRPS for RUV-III normalization. The shuffling steps were repeated ten times for each proportion, and the results were averaged for normalization performance assessments.

The results show that, even with poorly chosen PRPS, RUV-III outperforms the FPKM and FPKM.UQ normalization in terms of removing large library size differences and preserving the CMS clusters in the TCGA READ RNA-seq data (Supplementary Fig. 34a,b). The correlations between two pairs of genes, *MDH2{EIF4H}* and *TMF1\_BCLAF1* (Fig. 3), were also preserved in the RUV-III datasets with poorly chosen PRPS (Supplementary Fig. 34c). Furthermore, the association between *RAB18* gene expression and the survival outcome (Fig. 4) was identified in all the RUV-III datasets with poorly chosen PRPS. However, we found this association for the *FBXL14* gene only in RUV-III with 20% shuffled labels (Supplementary Fig. 34d).

We performed a similar analysis on the TCGA BRCA RNA-seq data. Our results showed that the RUV-III normalizations with poorly chosen PRPS also show satisfactory performance compared to both FPKM and FPKM.UQ in terms of removing the flow cell chemistry and tumor purity effects. However, RUV-III with 60% and 80% shuffled labels show a slightly lower performance compared to FPKM and FPKM.UQ normalization regarding the separation of the PAM50 subtypes (Supplementary Fig. 35). The gene–gene correlations and association between gene expression and survival outcomes demonstrated that the RUV-III normalizations

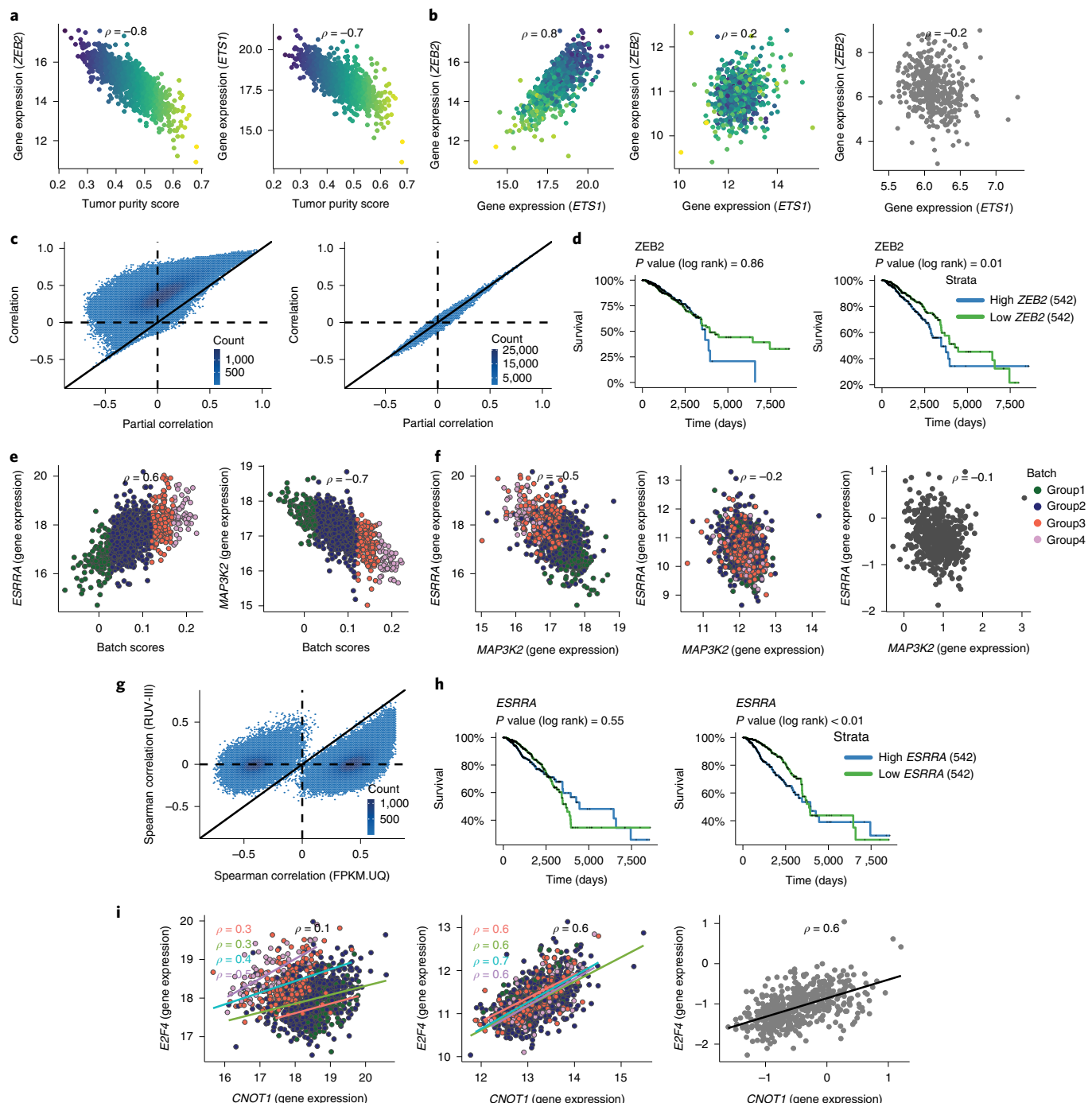


**Fig. 7 | Impact of tumor purity and flow cell chemistry variation on gene co-expression and survival analysis in the TCGA BRCA RNA-seq data.**

**a**, Relationship between tumor purity scores and the *ZEB2* and *ETS1* gene expression in the FPKM data. **b**, Scatter plots exhibit relationship between the *ZEB2* and *ETS1* gene expression in the FPKM data (left), the RUV-III normalized data (middle) and the LCM microarray data (right). **c**, Scatter plots show the Spearman correlation coefficients and partial correlation coefficients for all possible pairs of the genes that have the 1,300 highest correlations with tumor purity in the TCGA FPKM.UQ (left) and RUV-III normalized data (right). **d**, Kaplan-Meier survival analysis shows the association between the *ZEB2* gene expression and overall survival in the FPKM.UQ (left) and the RUV-III normalized data (right). **e**, Relationship between the *ESSRA* and *MAP3K2* gene expression with the batch scores in the FPKM.UQ data. **f**, Scatter plots show the relationship between the *ESSRA* and *MAP3K2* gene expression in the FPKM.UQ (left), the RUV-III normalized data (middle) and the TCGA BRCA microarray data (right). **g**, Scatter plots display Spearman correlation coefficients of all possible pairs of genes that are highly affected by flow cell chemistries in the FPKM.UQ and the RUV-III normalized data. **h**, Kaplan-Meier survival analysis shows the association between the *ESSRA* gene expression and overall survival in the FPKM.UQ (left) and the RUV-III normalized data (right). **i**, Scatter plots exhibit the relationship between the *E2F4* and *CNOT1* gene expression in the FPKM.UQ (left), the RUV-III normalized data (middle) and the TCGA BRCA microarray data (right).

with poorly chosen PRPS results in satisfactory normalization (Supplementary Fig. 35d–f).

Overall, our results illustrate that RUV-III shows a very satisfactory performance in a situation where PRPS is poorly chosen.

#### Performance of RUV-III with partially known biological labels.

We assessed the performance of RUV-III with PRPS in situations where the biological labels are partially known (hereafter called the RUV-III-P). To simulate such situations, we used one of the CMS subtypes, CMS4, to create PRPS for RUV-III normalization of the TCGA READ RNA-seq data. Note that this subtype is not present across all the plates. Our results clearly show that RUV-III-P normalization led to very satisfactory normalization by removing the large library size differences and plate effects and also preserving the CMS clusters (Supplementary Fig. 36). RUV-III-P also preserved the association between *RAB18* gene expression and survival outcomes in the TCGA READ RNA-seq data. However, this normalization did not show the same result for the *FXBL14* gene. This might be explained by the presence of the CMS4 subtype in eight out of 14 plates in the TCGA READ RNA-seq data.

Similar analyses were performed on the TCGA BRCA RNA-seq data. We used the basal and luminal A subtypes to create PRPS. The results demonstrated that performance of RUV-III-P was largely similar to the initial RUV-III normalization, in which all the PAM50 subtypes were used for producing PRPS (Supplementary Fig. 37).

These analyses show that RUV-III with PRPS can be used for normalization of RNA-seq data in situations where the biological labels of samples are only partially known.

#### Discussion

The main goal of RNA-seq normalization is to remove unwanted variation that can compromise downstream analyses while preserving biological variation. A suitable normalization method for cancer RNA-seq data must be able to remove unwanted variation introduced by sample library size differences, tumor purity (where appropriate), batch effects and other technical variation in data.

We proposed an approach, called PRPS, to deploy RUV-III for normalization of RNA-seq in situations where suitable technical replicates are not available. Our PRPS approach requires the presence of at least a homogenous biological population across sources of unwanted variation. Then, we create pseudo-samples by averaging gene expression of a group of samples that are roughly homogeneous regarding the unwanted variation and biology. The gene expression differences between pseudo-samples are mainly unwanted variation. These samples will be used by RUV-III as a set of pseudo-replicates to estimate one aspect of unwanted variation in the data.

We made use of three TCGA RNA-seq studies to compare the performance of RUV-III with PRPS with the state-of-art normalizations proposed for RNA-seq data. RUV-III is not limited to TCGA data normalization, and we have also shown that the method can be used to normalize RNA-seq data, when the data come from multiple studies. Our comparisons are based on statistical summaries, biological positive and negative controls and concordance with the corresponding TCGA or independent microarray studies.

We began by carefully identifying different known sources of unwanted variation in all the TCGA RNA-seq raw count, FPKM and FPKM.UQ normalized datasets. We illustrated that library size, tumor purity and plate or time effects are major sources of unwanted variation in these studies, and we showed how they can influence downstream analyses. These unwanted variations are likely to affect other downstream analyses not investigated in this study.

In the TCGA READ RNA-seq study, noticeable library size differences between samples remained in the FPKM and FPKM.UQ normalized data due to the presence of genes whose raw counts showed weak or negative association with library size. In such situations, normalizations that rely on a global scale factor can introduce,

rather than remove, library size variation. We found this issue in several TCGA cancer studies, even those that used a single plate for profiling. We took advantage of the gene-wise normalization ability of RUV-III to remove library size effects only from genes that are affected by this variation. Our results showed that RUV-III with PRPS effectively removed the library size effects from the TCGA READ RNA-seq data and led to better downstream analyses of gene–gene co-expression and association of gene expression with survival. Furthermore, the results showed that the variation due to tumor purity was highly similar for the TCGA and the RUV-III normalized datasets, as we did not attempt to remove the variation. This demonstrates the ability of RUV-III with PRPS approach to remove just the sources of unwanted variation that users aim to remove.

We found that the TCGA COAD RNA-seq data are affected by the same sources of unwanted variation that were identified in the corresponding READ RNA-seq data, although their effects were less severe in the COAD data compared to the READ data. The first two PCs of the FPKM and FPKM.UQ dataset did not show that the library size effects have not been properly removed. This highlights the importance of gene-level examinations to assess the performance of normalizations.

In the TCGA BRCA RNA-seq data, we designed our PRPS to remove variation in tumor purity as well as other sources of unwanted variation, including library size, flow cell chemistry and plate effects. We used LCM gene expression data to demonstrate the effects of tumor purity on the PAM50 subtype identification and gene co-expression analysis in the FPKM.UQ normalized data. We identified that the use of two flow cell chemistries introduced unwanted variation into the TCGA BRCA RNA-seq data. This introduced correlations between genes that were not truly associated and obscured the correlation between genes that were truly associated. We used the TCGA microarray data as an orthogonal platform to compare the gene expression patterns and their correlations in differently normalized datasets. The results of this comparison showed that the agreement between the RUV-III normalized data and the microarray data was much better than that found with the two TCGA normalized datasets.

The performance of RUV-III with the PRPS approach relies on the identification of major gene-expression-based biological populations in the data. Our results clearly showed that a rough identification of such populations using inadequate normalizations is satisfactory for creating the PRPS. In the three TCGA RNA-seq studies used in this study, the major biological populations were identified using TCGA normalized data that included sources of unwanted variation. However, we observed an equally good performance of RUV-III with PRPS using the biological populations identified in the RUV-III normalized data as we did using TCGA normalized data. Furthermore, we demonstrated that RUV-III is reasonably robust to poorly chosen PRPS.

Note that we could have created the PRPS using adjacent normal tissue, which is more homogeneous than cancer tissue, had these samples been more uniformly distributed across batches. However, we were not able to use such samples to create PRPS across the two flow cell chemistries for the BRCA study, as all 94 adjacent normal breast tissue samples were profiled using just one of the two chemistries. We found the same problem for the TCGA READ and COAD RNA-seq data. In these datasets, all normal adjacent tissues were profiled within a key time interval. It should be also noted that tumor purity is essentially the same across any set of technical replicates; thus, these samples are not useful to estimate and remove variation in tumor purity by the RUV-III normalization.

In large-scale genomics studies such as TCGA, samples are inevitably profiled using different reagents and platforms at different times, which can introduce unwanted variation into the data. As such, we strongly recommend including technical replicates across any possible source of unwanted variation. These samples can be

used by any technical-based normalizations and considered as positive control to assess of any normalizations. We also recommend distributing the biology of interests across batches, to the extent that this is possible, as this will assist the use of RUV-III with PRPS. However, as it is difficult to predict all sources of unwanted variation and appropriately design technical replicates across them, RUV-III with PRPS provides a tool to remove this unwanted variation from large-scale cancer and genomics studies.

## Online content

Any methods, additional references, Nature Research reporting summaries, source data, extended data, supplementary information, acknowledgements, peer review information; details of author contributions and competing interests; and statements of data and code availability are available at <https://doi.org/10.1038/s41587-022-01440-w>.

Received: 19 February 2022; Accepted: 30 June 2022;

Published online: 15 September 2022

## References

1. Risso, D. et al. Normalization of RNA-seq data using factor analysis of control genes or samples. *Nat. Biotechnol.* **32**, 896–902 (2014).
2. Robinson, M. D. & Oshlack, A. A scaling normalization method for differential expression analysis of RNA-seq data. *Genome Biol.* **11**, R25 (2010).
3. Bullard, J. H. et al. Evaluation of statistical methods for normalization and differential expression in mRNA-seq experiments. *BMC Bioinformatics* **11**, 94 (2010).
4. Risso, D. et al. GC-content normalization for RNA-seq data. *BMC Bioinformatics* **12**, 480 (2011).
5. Peixoto, L. et al. How data analysis affects power, reproducibility and biological insight of RNA-seq studies in complex datasets. *Nucleic Acids Res.* **43**, 7664–7674 (2015).
6. Leek, J. T. et al. Tackling the widespread and critical impact of batch effects in high-throughput data. *Nat. Rev. Genet.* **11**, 733–739 (2010).
7. Gagnon-Bartsch, J. A. & Speed, T. P. Using control genes to correct for unwanted variation in microarray data. *Biostatistics* **13**, 539–552 (2012).
8. Molania, R. et al. A new normalization for Nanostring nCounter gene expression data. *Nucleic Acids Res.* **47**, 6073–6083 (2019).
9. Dillies, M. A. et al. A comprehensive evaluation of normalization methods for Illumina high-throughput RNA sequencing data analysis. *Brief. Bioinform.* **14**, 671–683 (2013).
10. Lovén, J. et al. Revisiting global gene expression analysis. *Cell* **151**, 476–482 (2012).
11. Bacher, R. et al. SCnorm: robust normalization of single-cell RNA-seq data. *Nat. Methods* **14**, 584–586 (2017).
12. Hafemeister, C. & Satija, R. Normalization and variance stabilization of single-cell RNA-seq data using regularized negative binomial regression. *Genome Biol.* **20**, 296 (2019).
13. Beck, A. H. et al. Systematic analysis of breast cancer morphology uncovers stromal features associated with survival. *Sci. Transl. Med.* **3**, 108ra113 (2011).
14. Zhang, C. et al. Tumor purity as an underlying key factor in glioma. *Clin. Cancer Res.* **23**, 6279–6291 (2017).
15. Zhang, L. et al. Intratumoral T cells, recurrence, and survival in epithelial ovarian cancer. *N. Engl. J. Med.* **348**, 203–213 (2003).
16. Sato, E. et al. Intraepithelial CD8<sup>+</sup> tumor-infiltrating lymphocytes and a high CD8<sup>+</sup>/regulatory T cell ratio are associated with favorable prognosis in ovarian cancer. *Proc. Natl Acad. Sci. USA* **102**, 18538–18543 (2005).
17. Aran, D., Sirota, M. & Butte, A. J. Systematic pan-cancer analysis of tumour purity. *Nat. Commun.* **6**, 8971 (2015).
18. Yoshihara, K. & Verhaak, R. G. Hiding in the dark: uncovering cancer drivers through image-guided genomics. *Genome Biol.* **15**, 563 (2014).
19. Petralia, F. et al. A new method for constructing tumor specific gene co-expression networks based on samples with tumor purity heterogeneity. *Bioinformatics* **34**, i528–i536 (2018).
20. Ritchie, M. E. et al. limma powers differential expression analyses for RNA-sequencing and microarray studies. *Nucleic Acids Res.* **43**, e47 (2015).
21. Johnson, W. E., Li, C. & Rabinovic, A. Adjusting batch effects in microarray expression data using empirical Bayes methods. *Biostatistics* **8**, 118–127 (2007).
22. Zhang, Y., Parmigiani, G. & Johnson, W. E. ComBat-seq: batch effect adjustment for RNA-seq count data. *NAR Genom. Bioinform.* **2**, lqaa078 (2020).
23. Gandolfo, L. C. & Speed, T. P. RLE plots: visualizing unwanted variation in high dimensional data. *PLoS ONE* **13**, e0191629 (2018).
24. Guinney, J. et al. The consensus molecular subtypes of colorectal cancer. *Nat. Med.* **21**, 1350–1356 (2015).
25. Eide, P. W. et al. CMScaller: an R package for consensus molecular subtyping of colorectal cancer pre-clinical models. *Sci. Rep.* **7**, 16618 (2017).
26. Zhou, X. et al. BCALF1 and its splicing regulator SRSF10 regulate the tumorigenic potential of colon cancer cells. *Nat. Commun.* **5**, 4581 (2014).
27. Chen, Z. H. et al. Eukaryotic initiation factor 4A2 promotes experimental metastasis and oxaliplatin resistance in colorectal cancer. *J. Exp. Clin. Cancer Res.* **38**, 196 (2019).
28. Ban, H. S. et al. A novel malate dehydrogenase 2 inhibitor suppresses hypoxia-inducible factor-1 by regulating mitochondrial respiration. *PLoS ONE* **11**, e0162568 (2016).
29. Zhong, K. et al. MicroRNA-30b/c inhibits non-small cell lung cancer cell proliferation by targeting Rab18. *BMC Cancer* **14**, 703 (2014).
30. Song, Y. et al. Emerging role of F-box proteins in the regulation of epithelial–mesenchymal transition and stem cells in human cancers. *Stem Cell Res. Ther.* **10**, 124 (2019).
31. Martinez-Romero, J. et al. Survival marker genes of colorectal cancer derived from consistent transcriptomic profiling. *BMC Genomics* **19**, 857 (2018).
32. Foroutan, M. et al. Single sample scoring of molecular phenotypes. *BMC Bioinformatics* **19**, 404 (2018).
33. di Gennaro, A. et al. Correction to: A p53/miR-30a/ZEB2 axis controls triple negative breast cancer aggressiveness. *Cell Death Differ.* **26**, 2493 (2019).
34. Comijn, J. et al. The two-handed E box binding zinc finger protein SIP1 downregulates E-cadherin and induces invasion. *Mol. Cell.* **7**, 1267–1278 (2001).
35. Yalim-Camci, I. et al. ETS1 is coexpressed with ZEB2 and mediates ZEB2-induced epithelial–mesenchymal transition in human tumors. *Mol. Carcinog.* **58**, 1068–1081 (2019).
36. Kim, G. C. et al. ETS1 suppresses tumorigenesis of human breast cancer via trans-activation of canonical tumor suppressor genes. *Front. Oncol.* **10**, 642 (2020).
37. Toro, A. L. et al. Effect of obesity on molecular characteristics of invasive breast tumors: gene expression analysis in a large cohort of female patients. *BMC Obes.* **3**, 22 (2016).
38. Fang, Y. et al. Protein expression of ZEB2 in renal cell carcinoma and its prognostic significance in patient survival. *PLoS ONE* **8**, e62558 (2013).
39. Goossens, S. et al. ZEB2 drives immature T-cell lymphoblastic leukaemia development via enhanced tumour-initiating potential and IL-7 receptor signalling. *Nat. Commun.* **6**, 5794 (2015).
40. Zheng, J. Is SATB1 a master regulator in breast cancer growth and metastasis? *Womens Health* **4**, 329–332 (2008).
41. Riabov, V. et al. Stabilin-1 is expressed in human breast cancer and supports tumor growth in mammary adenocarcinoma mouse model. *Oncotarget* **7**, 31097–31110 (2016).
42. Hollmén, M., Figueiredo, C. R. & Jalkanen, S. New tools to prevent cancer growth and spread: a 'Clever' approach. *Br. J. Cancer* **123**, 501–509 (2020).
43. Perou, C. M. et al. Molecular portraits of human breast tumours. *Nature* **406**, 747–752 (2000).
44. Parker, J. S. et al. Supervised risk predictor of breast cancer based on intrinsic subtypes. *J. Clin. Oncol.* **27**, 1160–1167 (2009).
45. Cheang, M. C. et al. Defining breast cancer intrinsic subtypes by quantitative receptor expression. *Oncologist* **20**, 474–482 (2015).
46. Harbeck, N. et al. Breast cancer. *Nat. Rev. Dis. Primers* **5**, 66 (2019).
47. Weigelt, B. et al. Breast cancer molecular profiling with single sample predictors: a retrospective analysis. *Lancet Oncol.* **11**, 339–349 (2010).
48. Bastien, R. R. et al. PAM50 breast cancer subtyping by RT-qPCR and concordance with standard clinical molecular markers. *BMC Med. Genomics* **5**, 44 (2012).
49. Brueffler, C. et al. Clinical value of RNA sequencing-based classifiers for prediction of the five conventional breast cancer biomarkers: a report from the population-based multicenter Sweden Cancerome Analysis Network-Breast Initiative. *JCO Precis. Oncol.* **2**, PO.17.00135 (2018).
50. Brueffler, C. et al. The mutational landscape of the SCAN-B real-world primary breast cancer transcriptome. *EMBO Mol. Med.* **12**, e12118 (2020).
51. Ringnér, M. et al. GOBO: gene expression-based outcome for breast cancer online. *PLoS ONE* **6**, e17911 (2011).

**Publisher's note** Springer Nature remains neutral with regard to jurisdictional claims in published maps and institutional affiliations.



**Open Access** This article is licensed under a Creative Commons Attribution 4.0 International License, which permits use, sharing, adaptation, distribution and reproduction in any medium or format, as long as you give appropriate credit to the original author(s) and the source, provide a link to the Creative Commons license, and indicate if changes were made. The images or other third party material in this article are included in the article's Creative Commons license, unless indicated otherwise in a credit line to the material. If material is not included in the article's Creative Commons license and your intended use is not permitted by statutory regulation or exceeds the permitted use, you will need to obtain permission directly from the copyright holder. To view a copy of this license, visit <http://creativecommons.org/licenses/by/4.0/>.

© The Author(s) 2022

## Methods

**Datasets.** The TCGA consortium aligned RNA-seq reads to the hg38 reference genome using STAR aligner and quantified the results at gene level using HTSeq and GENCODE version 22 gene annotation<sup>52</sup>. The TCGA RNA-seq data are publicly available in three formats: raw counts, FPKM and FPKM\_UQ. All these formats for individual cancer types (33 cancer types, ~11,000 samples) were downloaded using the R/Bioconductor package TCGAAbiolinks (version 2.16.1)<sup>53</sup>. The TCGA normalized microarray gene expression data were downloaded from the Broad GDAC Firehose repository (<https://gdac.broadinstitute.org>), data version 2016/01/28. TSSs and batches of sequencing plates were extracted from individual TCGA patient barcodes ([https://docs.gdc.cancer.gov/Encyclopedia/pages/TCGA\\_Barcodes/](https://docs.gdc.cancer.gov/Encyclopedia/pages/TCGA_Barcodes/)), and sample processing times were downloaded from the MD Anderson Cancer Center TCGA Batch Effects website: <https://bioinformatics.mdanderson.org/public-software/tcgabatch-effects>. Pathological features of patients with cancer were downloaded from the Broad GDAC Firehose repository (<https://gdac.broadinstitute.org>). The details of processing the TCGA BRCA RNA-seq samples using two flow cell chemistries were received by personal communication from Dr. Katherine Hoadley. The TCGA survival data reported by Liu et al.<sup>54</sup> were used in this paper. The breast cancer LCM microarray dataset was downloaded using the GEOquery R/Bioconductor package (version 2.62.2) from the National Center of Biotechnology Information (NCBI) Gene Expression Omnibus (GSE78958 (ref. 37)). The two non-TCGA RNA-seq datasets were downloaded from the NCBI Gene Expression Omnibus with accession numbers GSE96058 and GSE81538 (refs. 49,50). The consensus measurement of purity estimation (CPE) was downloaded from the Aran et al. study<sup>17</sup>.

**Filtering samples and genes.** We applied the following filtering steps to the individual TCGA RNA-seq datasets. Plates with fewer than three samples were removed. Samples with log<sub>2</sub> library sizes of three median absolute deviations lower than the median of all log<sub>2</sub> library sizes were excluded from the data.

The R/Bioconductor package biomaRt (version 2.48.3) was used to annotate genes. All pseudo-genes and immunoglobulin genes were excluded. For the pan-cancer analyses, we retained genes with at least 15 raw read counts in at least 20% of samples. We considered numbers of samples in the biological subpopulations and sources of unwanted variation when removing lowly expressed genes in the TCGA READ, COAD and BRCA data. To do so, we kept genes that have at least 15 counts in the smallest biological subpopulations within each of the key time intervals in the datasets.

**Tumor purity estimates.** We estimated tumor purity for all TCGA RNA-seq cancer samples using the stromal and immune gene signatures (Supplementary Table 1) from the Yoshihara et al. study<sup>55</sup> and the R/Bioconductor package singscore version (1.12.0)<sup>32</sup>. The stromal-immune scores were transformed to 1-stromal-immune scores for downstream analyses. These measurements are called tumor purity scores in this study. The tumor purity scores showed high positive correlation (mean = 0.95, Pearson correlation) with the ESTIMATE measurements from the Aran et al. study<sup>17</sup> (Supplementary Fig. 38).

**Sample library size.** Sample library sizes were obtained by adding all gene raw counts for individual samples after removing pseudo-genes, immunoglobulin and lowly expressed genes. All sample library sizes are transformed to log<sub>2</sub> in this study.

**RUV-III normalization.** Before we can describe the linear model underlying RUV-III, we need to introduce the  $m \times m_1$  mapping matrix  $M$  connecting assays to distinct samples, which captures the pattern of replication in our assays. Here,  $m$  is the number of assays, and  $m_1$  is the number of distinct samples being assayed.  $M(i, h) = 1$  if assay  $i$  is on sample  $h$  and  $M(i, h) = 0$  otherwise. Each row of  $M$  sums to 1, and the columns sum to the distinct sample replication numbers, the elements of  $M^T M$ . We also define an  $m_1 \times p$  design matrix  $X$  to capture the biological factor(s) of interest indexed by sample rather than assay. There are no constraints on  $p$ ; indeed,  $X$  could be the  $m_1 \times m_1$  identity matrix. Our goal here is to remove unwanted variation, not to estimate regression parameters.

The linear model we use is:

$$Y = 1\mu + MX\beta + W\alpha + \epsilon$$

where the data  $Y = (y_{ij})$  and unobserved errors  $\epsilon = (\epsilon_{ij})$  are  $m \times n$ ; the matrices  $X$  and  $M$  have just been defined;  $\mu$  is the  $1 \times n$  row of gene means;  $\beta$  is  $p \times n$ ; the matrix  $W$  whose columns capture the unwanted variation is  $m \times k$ ; and  $\alpha$  is  $k \times n$ .  $1 = 1_{m_1}$  is the  $m_1 \times 1$  column vector of 1s. Here,  $m$  = number of assays,  $n$  = number of genes and  $p$  is the dimension of the wanted variation  $X$  and  $k$  that of the unwanted variation  $W$ . Assume that  $W \perp 1$ .

Also, we suppose that we have a subset of  $n_c$  of negative control genes whose  $m \times n_c$  submatrix  $Y_c$  satisfies  $Y_c = 1\mu_c + W\alpha_c + \epsilon_c$ , where we have assumed that  $\beta_c = 0$ —that is, that there is no true association between these genes and the biology of interest.

The projection  $P_M = M(M^T M)^{-1}M^T$  replaces each entry  $y_{ij}$  of  $Y$  by the simple average of the entries  $y_{ij}$  over all  $i'$  for which  $M(i, h) = M(i', h) = 1$ —that is,

over all  $i'$  such that  $i'$  and  $i$  label replicate assays of the same unique sample (or pseudo-sample) labeled  $h$ .

Write  $R_M = I - P_M$  for the corresponding residual projector. This is our source of information on the unwanted variation that we will remove. If the replication is technical at some level, then  $R_M Y$  mainly contains information about unwanted variation in the system after the technical replicates were created. Depending on the study details, technical replicates could be created immediately before the assay was run, in parallel with or immediately after sample was collected or somewhere in between. The earlier the creation of technical replicates, the more unwanted variation will be captured in their differences. The use of pseudo-replicates of suitable pseudo-samples enables us to start to deal with pre-technical unwanted variation.

Write the spectral decomposition of  $R_M Y Y^T R_M = U D U^T$ , where  $U$  is an  $m \times m$  orthogonal matrix and  $D$  is an  $m \times n$  diagonal matrix with entries ordered from largest to smallest eigenvalue. Let  $P_1$  be the orthogonal projection onto  $1_{m_1}$ .

For a chosen  $k$ ,  $1 \leq k \leq m - m_1$ ,

- I. Define  $\hat{\alpha}^{(k)} = U^{(k)T} Y$ , where  $U^{(k)}$  is the first  $k$  columns of  $U$
- II. Estimate  $W$  by regressing the centered negative controls  $(I - P_1) Y_c$  on  $\hat{\alpha}_c^{(k)T}$

$$\hat{W}^{(k)} = (I - P_1) Y_c \left( U^{(k)T} Y_c \right)^T \left[ \left( U^{(k)T} Y_c \right) \left( U^{(k)T} Y_c \right)^T \right]^{-1}$$

Finally, we:

- III. Form the adjusted/normalized  $Y$ ,  $Y^{(k)} = Y - \hat{W}^{(k)} \hat{\alpha}^{(k)}$ .

**PRPS.** We used our recently developed normalization method, RUV-III, which makes essential use of technical replicates and negative control genes, to estimate unwanted variation and remove it from the data<sup>8</sup>. Ideally, technical replicates are placed across batches so that unwanted variation between any pair of batches is captured via differences of expression values between technical replicates. We previously showed the performance of RUV-III with pseudo-replicates in removing unwanted variation from gene expression data. Pseudo-replicates are samples from the same biological groups across batches. The idea of pseudo-replicates has also been used to remove batch effects in TCGA RNA-seq data with the unpublished algorithm EB++<sup>36</sup>.

As there are no technical replicates in the TCGA RNA-seq datasets, we developed an approach, PRPS, to be able to use RUV-III to remove unwanted variation from the data. To use RUV-III with PRPS, we first need to find sources of unwanted variation that we aim to remove from the data and identify relatively homogenous biological subpopulations among the samples. Then, we build pseudo-samples, which are *in silico* samples derived from a group of samples that are roughly homogeneous with respect to the unwanted variation and biology. The pseudo-samples from each biological groups will be a set of pseudo-replicates.

To make the process clear, we illustrate the PRPS for TCGA COAD and BRCA RNA-seq studies. For example, with the TCGA COAD samples, we regarded the 12 combinations of four CMSs (CMS1, CMS2, CMS3 and CMS4) with three microsatellite instability (MSI) statuses (MSI-high, MSI-low and MS-stable) as defining biological subpopulations. The key time intervals 2010 and 2011–2014 contribute the main unwanted variation that we saw after preliminary exploration of the data. As these times are totally confounded with sequencing plates (that is, different plates are used across different times), we considered plates to be the batches when defining PRPS. In addition, we were able to remove plate effects within each key time interval. As a result, to remove unwanted variation from the COAD data without removing biology, we created sets of pseudo-samples as follows: (1) select those biological subpopulations out of the 12 mentioned above that have at least three samples in at least two plates while also ensuring that, in the end, there are samples from plates within and across the two key intervals; and (2) average the gene expression levels of the corresponding samples within the individual plates to create one pseudo-sample. Having done this for all 12 biological subpopulations, we suppose all the pseudo-samples created across plates for a particular biological subpopulation to form a pseudo-replicate set.

For the BRCA data, we aimed to remove four different sources of unwanted variation—library size, tumor purity, flow cell chemistry and plate effects—from the data. Then, we needed to create distinct groups of PRPS for each source of unwanted variation. Note that we created a group of PRPS to remove the effects of plates and flow cell chemistries, as they are completely confounded with each other.

We considered the PAM50 subtypes (basal, Her2, luminal A, luminal B and normal-like) to define the major biological subpopulations and then created several sets of PRPS for each source of unwanted variation. To create PRPS for library size, we selected plates that have at least 12 samples of a particular PAM50 subtype and then selected the samples with the three highest and the samples with the three lowest values of library size. Then, we created two pseudo-samples within each PAM50 subtype per plate by averaging the gene expression values across each set of three high library size samples and each set of three low library size samples. We adopted the same approach explained above for the COAD data to create PRPS for plate effects. For removing the effect of tumor purity in the BRCA data, we defined sets of PRPS for each PAM50 subtype in addition to those that we created

for removing library size, flow cell chemistries and plate-to-plate variation. We performed this by selecting the samples with the three highest and the samples with the three lowest values of tumor purity within each PAM50 subtype. Then, we created two pseudo-samples within each PAM50 subtype by averaging the gene expression values across each set of three high-purity samples and each set of three low-purity samples. Finally, the two pseudo-samples (average high and average low purity) created for each PAM50 subtype were regarded as forming a pseudo-replicate set—that is, a pair of pseudo-duplicates.

**Choice of negative control genes and K.** Negative control genes for RUV-III are genes that are not highly affected by the biological factors of interest but are affected by one or more forms of unwanted variation in the data. We previously<sup>8</sup> explained that our approach to negative controls is pragmatic: if regarding a set of genes as negative controls helps to remove unwanted variation using RUV-III, as evaluated by various metrics, then whether or not they are ideal negative control genes is not our concern. For the different cancer types discussed in this paper, we used different sets of negative control genes derived from either the literature (for example, housekeeping genes or genes found to be stable in the same, or a closely related, biological context) or the data itself (for example, genes found to exhibit little or no biological, but clear unwanted, variation). Candidate control genes have their effectiveness evaluated using various metrics after their use in RUV-III. It should be noted that unwanted variation mostly affects different subsets of genes in different ways.

To use RUV-III, a dimension  $K$  of unwanted variation needs to be determined. To find a suitable value, we repeated the analysis with a range of values of  $K$  and evaluated the quality of each analysis using different statistical metrics and prior biological knowledge. RUV-III is generally robust to overestimating  $K$  but not always.

**RUUV-III normalization with PRPS for READ.** As described above, the 11 combinations (we do not have CMS4\_MSI-H) of the four CMS subtypes identified by the R package CMScaller on the READ FPKM and FPKM.UQ RNA-seq data (consensus calls were selected), and the three MSI statuses, were considered to be homogenous biological populations for the purpose of creating PRPS. Supplementary Fig. 39 displays the numbers of each 11 subpopulations within the individual plates. We created pseudo-samples from plates that have at least two samples of at least one of the 11 subpopulations. Supplementary Fig. 39b shows the library size of pseudo-samples within each subpopulation.

A set of negative control genes was selected in the following way. First, an ANOVA was carried out on FPKM.UQ normalized gene expression levels using the consensus calls of CMS subtypes as the factor, and the genes with lowest  $F$ -statistics were selected (~1,000 genes). PCA plots of the READ RNA-seq raw counts using the negative control genes showed that they capture the large library size differences between the key time intervals and do not capture CMS subtype differences (Supplementary Fig. 39c).

**RUUV-III normalization with PRPS for COAD.** Here we first defined CMS using the R package CMScaller on the COAD FPKM and FPKM.UQ RNA-seq data and selected the samples receiving the same CMS call for both (406 out of 479 samples). We used these CMSs and MSIs to define homogenous biological populations for the purpose of creating the PRPS (Supplementary Fig. 40). We used a slightly complicated approach to select a suitable set of negative control genes for the COAD study as follows: (1) carry out an ANOVA on the FPKM.UQ normalized gene expression values with CMS subtypes as the factor; (2) calculate Spearman correlations between FPKM.UQ normalized gene expression values and tumor purity; (3) calculate Spearman correlations between FPKM.UQ normalized gene expression values and the average expression level of a set of housekeeping genes<sup>57</sup>; and then (4) select genes (262 genes) that have lowest  $F$ -statistics ( $F$ -statistics  $< 20$ ) from (1), the lowest correlations ( $\rho < 0.3$ ) from (2) and the highest correlations ( $\rho > 0.9$ ) from (3). PCA plots of the TCGA COAD RNA-seq raw count using negative control genes show that they capture the key time differences (Supplementary Fig. 40c).

**RUUV-III normalization with PRPS for BRCA.** The PAM50 subtypes were identified by using the R package genefu<sup>58</sup> with the FPKM and FPKM.UQ normalized data. We selected samples with consensus PAM50 subtypes from the two datasets for creating PRPS. Three different groups of PRPS were then created to capture the library size, plate and flow cell chemistries and tumor purity effects (Supplementary Fig. 41).

The negative control genes were selected as follows: (1) carry out an ANOVA on the FPKM.UQ normalized gene expression values with PAM50 subtype as the factor, within each flow cell chemistry; (2) carry out a similar ANOVA with flow cell chemistry as the factor; (3) calculate Spearman correlations between FPKM.UQ normalized gene expression and purity values within the PAM50 subtypes; (4) calculate similar Spearman correlations with library size but with the raw counts; (5) select genes (4,500 genes) with the lowest  $F$ -statistics ( $F$ -statistics  $< 20$ ) from (1), the highest  $F$ -statistics ( $F$ -statistics  $> 100$ ) from (2), the highest correlations ( $|\rho| > 0.7$ ) from (3) and the highest correlations ( $\rho > 0.07$ ) from (4). PCA plots of the TCGA BRCA RNA-seq raw count using the negative control genes show that these genes capture all sources of unwanted variation in the data (Supplementary Fig. 42c).

**Other RNA-seq normalization methods.** We did not include the SVAseq<sup>59</sup>, ComBat-seq<sup>22</sup> and RUVg<sup>1</sup> methods in our analysis as these are not specifically designed for normalization, although they can be helpful for that task when the unwanted variation is orthogonal to the biology, something that is rarely known in advance. The same applies to the RUVs method provided in the RUVseq package<sup>1</sup>. Although if there are true replicates (missing from TCGA and most large cancer RNA-seq studies), it can be used to normalize RNA-seq datasets<sup>5</sup>.

**PCA.** The PCs (in this context also called singular vectors) of the sample  $\times$  transcript array of log counts are the linear combinations of the transcript measurements having the largest, second largest, third largest, etc., variation, standardized to be of unit length and orthogonal to the preceding components. Each will give a single value for each sample. In this paper, PCA plots are of the second PC values versus the first PC values and of the third PC versus the first PC. The calculations are done on mean-corrected transcript log counts, using the R code adopted from the R package EDASEQ (version 2.26.1)<sup>4</sup>.

**RLE plots.** RLE plots<sup>23</sup> are used to reveal trends, temporal clustering and other non-random patterns resulting from unwanted variation in gene expression data. To generate RLE plots, we first formed the log ratio  $\log(y_g/y_{\bar{g}})$  of the raw count  $y_g$  for gene  $g$  in the sample labeled  $i$  relative to the median value  $y_{\bar{g}}$  of the counts for gene  $g$  taken across all samples. We then generated a box plot from all the log ratios for sample  $i$  and plotted all such box plots along a line, where  $i$  varies in a meaningful order, usually sample processing date. An ideal RLE plot should have its medians centered around zero, and its box widths and their interquartile ranges (IQRs) should be similar in magnitude. Because of their sensitivity to unwanted variation, we also examined the relationships between RLE medians with potential sources of unwanted variation and individual gene expression levels in the datasets. In the absence of any influence of unwanted variation in the data, we should see no such associations.

**Vector correlation.** We used the Rozeboom squared vector correlation<sup>60</sup> to quantify the strength of (linear) relationships between two sets of variables, such as the first  $k$  PCs (that is  $1 \leq k \leq 10$ ) and dummy variables representing time, batches, plates and biological variables. Not only does this quantity summarize the full set of canonical correlations, but it also reduces to the familiar  $R^2$  from multiple regression (see below) when one of the variable sets contains just one element.

**Linear regression.**  $R^2$  values of fitted linear models are used to quantify the strength of the (linear) relationships between a single quantitative source of unwanted variation, such as sample (log) library size or tumor purity, and global sample summary statistics, such as the first  $k$  PCs ( $1 \leq k \leq 10$ ). The lm() R function was used for this analysis.

**Partial correlation.** Partial correlation is used to estimate Pearson (linear) correlation between two variables while controlling for one variables<sup>61</sup>. We computed the partial correlation between the expression levels of pairs of genes controlling for tumor purity using the pcor.test() function from the R package ppcor (version 1.1)<sup>61</sup>.

**ANOVA.** ANOVA enables us to assess the effects of a given qualitative variable (which we call a factor) on gene expression measurements across any set of groups (labeled by the levels of the factor) under study. We use ANOVA  $F$ -statistics to summarize the effects of a qualitative source of unwanted variation (for example, batches) on the expression levels of individual genes, where genes having large  $F$ -statistics are deemed to be affected by the unwanted variation. We also use ANOVA tests (the aov() function in R) to assign  $P$  values to the association between tumor purity and molecular subtypes.

**P value histograms.** It has been shown by Leek and Storey<sup>62</sup> and others that histograms of the raw (that is, unadjusted)  $P$  values resulting from testing the same hypothesis (for example, of no differential expression across two or more groups of samples) on thousands of genes can be powerful indicator of the presence of unwanted variation. When there is no such variation and the underlying statistical model is appropriate, such  $P$  value histograms should be uniform apart from a possible peak near zero corresponding to genes where the null should be rejected. When there is unwanted variation, the histograms typically look very far from uniform apart from a peak near zero.

**Silhouette coefficient analysis.** We used silhouette coefficient analysis to assess the separation of biological populations and batch effects. The silhouette function uses Euclidean distance to calculate both the similarity between one patient and the other patients in each cluster and the separation between patients in different clusters. A better normalization method will lead to higher and lower silhouette coefficients for biological and batch labels, respectively. The silhouette coefficients were computed using the function silhouette() from the R package cluster (version 2.1.2)<sup>63</sup>.

**ARI.** The ARI<sup>64</sup> is the corrected-for-chance version of the Rand index. The ARI measures the percentage of matches between two label lists. We used the ARI to assess the performance of normalization methods in terms of sample subtype

separation and batch mixing. We first calculated PCs and used the first three PCs to perform ARI.

**DE analysis.** DE analyses were performed using the Wilcoxon signed-rank test with log<sub>2</sub>-transformed raw counts and normalized data<sup>65</sup>. To evaluate the effects of the different sources of unwanted variation on the data, DE analyses were performed across batches. In the absence of any batch effects, the histogram of the resulting unadjusted *P* values should be uniformly distributed. The *wilcox.test()* R function was used for this analysis.

**Identification of unwanted variation in TCGA RNA-seq datasets.** We made use of both global and gene-level approaches to identify and quantify unwanted variation in RNA-seq datasets (Extended Data Fig. 2). These approaches are also used to assess the performance of different normalization methods as removers of unwanted variation and preservers of biological variation in the data.

Our global approaches involve the use of PCA plots, linear regression, vector correlation analyses, silhouette coefficients, ARIs and RLE plots<sup>23</sup>. Our PCA plots (see above) are each of the first three PCs against each other, colored by known sources of unwanted variation—for example, time—or known biology—for example, cancer subtype. Linear regression is used to quantify the relationship between the first few PCs and continuous sources of unwanted variation, such as (log) library size. The *R*<sup>2</sup> calculated from the linear regression analyses indicates how strongly the PCs capture unwanted variation in the data, and we perform these calculations cumulatively—that is, continuous source versus all of (PC<sub>1</sub>, ..., PC<sub>k</sub>), for  $k = 1, \dots, 5$  or 10. Similarly to linear regression, we used vector correlation analysis to assess the effect on the data of discrete sources of unwanted variation, such as years or year intervals. Silhouette coefficients and ARIs were used to quantify how well experimental batches are mixed and known biology is separated. Finally, RLE plots<sup>23</sup> were used to assess the performance of different normalizations in terms of removing unwanted variation from the data. We also explored the relationship between the medians and the IQRs of the RLE plots with sources of unwanted variation.

The gene-level approach includes DE analyses between experimental batches, looking at *P* value histograms and assessing the expression levels of negative control genes (see above), positive control genes (genes whose behavior we know), Spearman correlation and ANOVA between individual gene expression and sources of unwanted variation. These methods assess and quantify the effects of unwanted variation on individual gene expression levels in the RNA-seq datasets. See Methods section for more details about the assessment tools.

**Cancer subtype identification.** We identified gene-expression-based cancer subtypes to create PRPS for RUV-III normalization. The *CMScaller()* function with default parameters from the R package *CMScaller* (version 2.0.1)<sup>25</sup> was used to identify the CMSs in the TCGA READ and COAD RNA-seq data. The function provides classification based on pre-defined cancer-cell-intrinsic CMS templates.

We used two approaches to identify the PAM50 subtypes in the TCGA BRCA RNA-seq data. We implemented an algorithm proposed by Picornell et al.<sup>66</sup> on the estrogen receptor (ER) balanced data. The ER estimates = 1.4 were selected to divide samples into ER-positive and ER-negative groups, and then the calibration (median normalization) factors were calculated.

In addition, we also used the *molecular.subtyping()* function with the PAM50 (single sample predictor) model from the R/Bioconductor package *genefu* (version 2.26.0) to identify the PAM50 subtypes. This method performs Spearman correlation between the expression of the PAM50 genes of each sample and PAM50 centroids (these data were downloaded here: <https://github.com/bhklab/genefu>) to calculate the correlation coefficient for individual PAM50 subtypes. Then, the individual sample is assigned to a particular PAM50 subtype based on its highest correlation coefficient.

We used Kaplan–Meier survival analysis to assess the prognostic values of different PAM50 identification approaches. The results showed that the PAM50 subtypes obtained by the *genefu* method are slightly more prognostic than those obtained by the other method (Supplementary Fig. 27).

**Spurious gene–gene correlation.** We used two strategies to show spurious gene–gene correlations in the TCGA normalized data. First, we demonstrated how sources of unwanted variation, such as library size, tumor purity and batch effects, can introduce such correlations, which we did not see in the RUV-III normalized data. Second, we used the TCGA microarray gene expression data as orthogonal platform to explore and confirm these correlations. The TCGA microarray data contain gene expression data of subsets of samples that were profiled by RNA-seq platform. Our normalization assessment showed that the microarray data were not influenced by plates and time effects.

To explore spurious gene–gene correlations introduced by tumor purity in the TCGA data, we used the LCM microarray data, as these contain only gene expression signals from cancer cells. Note that we assessed both purity variation and quality of the LCM data.

**Reporting summary.** Further information on research design is available in the Nature Research Reporting Summary linked to this article.

## Data availability

The TCGA RNA-seq data are publicly available in three formats: raw counts, FPKM and FPKM.UQ. All these formats for individual cancer types (33 cancer types, ~11,000 samples) were downloaded using the R/Bioconductor package *TCGAbiolinks* (version 2.16.1). We have created summarized experiment objects containing expression data (raw counts, FPKM and FPKM.UQ), clinical and batch information and gene annotations for all the TCGA RNA-seq data. These files are deposited here: <https://zenodo.org/record/6326542#.YlN56y8Rquo> (ref. <sup>67</sup>). The TCGA microarray gene expression data level 3 were downloaded from the Broad GDAC Firehose repository: <https://gdac.broadinstitute.org>, data version 2016/01/28. TCGA sample processing times were downloaded from the MD Anderson Cancer Center TCGA Batch Effects website: <https://bioinformatics.mdanderson.org/public-software/tcga-batch-effects>. The TCGA survival data were downloaded from the Liu et al. study<sup>54</sup>. The CPEs were downloaded from the Aran et al. study<sup>17</sup>. The breast cancer LCM and two non-TCGA RNA-seq datasets were downloaded from the NCBI Gene Expression Omnibus, with accession numbers *GSE78958* (ref. <sup>37</sup>), *GSE96058* and *GSE81538* (refs. <sup>49,50</sup>) using the GEOquery R/Bioconductor package (version 2.62.2). The datasets that are required for the vignettes are deposited here: <https://zenodo.org/record/6392171#.YlN6Yi8Rquo>. The RUV-III normalized data of the TCGA READ, COAD and BRCA RNA-seq datasets are deposited here: <https://zenodo.org/record/6459560#.YldJ4S8Rquo> (ref. <sup>68</sup>).

## Code availability

We developed an RShiny application and the *tcgaCleaner* package to explore and remove unwanted variation in the TCGA RNA-seq datasets. All scripts were used to generate the main and supplementary figures, and two comprehensive vignettes that show all the steps in processing the TCGA READ and BRCA RNA-seq data are available on GitHub at: [https://github.com/RMolania/TCGA\\_PanCancer\\_UnwantedVariation](https://github.com/RMolania/TCGA_PanCancer_UnwantedVariation) (ref. <sup>69</sup>).

## References

52. Gao, G. F. et al. Before and after: comparison of legacy and harmonized TCGA genomic data commons' data. *Cell Syst.* **9**, 24–34 (2019).
53. Colaprico, A. et al. TCGAbiolinks: an R/Bioconductor package for integrative analysis of TCGA data. *Nucleic Acids Res.* **44**, e71 (2016).
54. Liu, J. et al. An integrated TCGA pan-cancer clinical data resource to drive high-quality survival outcome analytics. *Cell* **173**, 400–416 (2018).
55. Yoshihara, K. et al. Inferring tumour purity and stromal and immune cell admixture from expression data. *Nat. Commun.* **4**, 2612 (2013).
56. Hoadley, K. A. et al. Cell-of-origin patterns dominate the molecular classification of 10,000 tumors from 33 types of cancer. *Cell* **173**, 291–304 (2018).
57. Bhuva, D. D., Cursons, J. & Davis, M. J. Stable gene expression for normalisation and single-sample scoring. *Nucleic Acids Res.* **48**, e113 (2020).
58. Gendoo, D. M. et al. Genefu: an R/Bioconductor package for computation of gene expression-based signatures in breast cancer. *Bioinformatics* **32**, 1097–1099 (2016).
59. Leek, J. T. svaseq: removing batch effects and other unwanted noise from sequencing data. *Nucleic Acids Res.* **42**, e161 (2014).
60. Rozeboom, W. W. Linear correlations between sets of variables. *Psychometrika* **30**, 57–71 (1965).
61. Kim, S. ppcor: an R Package for a fast calculation to semi-partial correlation coefficients. *Commun. Stat. Appl. Methods* **22**, 665–674 (2015).
62. Leek, J. T. & Storey, J. D. Capturing heterogeneity in gene expression studies by surrogate variable analysis. *PLoS Genet.* **3**, 1724–1735 (2007).
63. Balzano, W. & Del Sorbo, M. R. Genomic comparison using data mining techniques based on a possibilistic fuzzy sets model. *Biosystems* **88**, 343–349 (2007).
64. Hubert, L. & Arabie, P. Comparing partitions. *J. Classif.* **2**, 193–218 (1985).
65. Robinson, M. D., McCarthy, D. J. & Smyth, G. K. edgeR: a Bioconductor package for differential expression analysis of digital gene expression data. *Bioinformatics* **26**, 139–140 (2010).
66. Picornell, A. C. et al. Breast cancer PAM50 signature: correlation and concordance between RNA-seq and digital multiplexed gene expression technologies in a triple negative breast cancer series. *BMC Genomics* **20**, 452 (2019).
67. Molania, R. TCGA\_PanCancerRNAseq. *Zenodo* <https://zenodo.org/record/6326542#.YlN56y8Rquo> (2022).
68. Molania, R. RUV-III-PRPS normalised data of the TCGA READ, COAD and BRCA RNA-seq studies. *Zenodo* <https://zenodo.org/record/6459560#.YlN6Yi8Rquo> (2022).
69. Molania, R. RMolania/TCGA\_PanCancer\_UnwantedVariation. *GitHub* [https://github.com/RMolania/TCGA\\_PanCancer\\_UnwantedVariation](https://github.com/RMolania/TCGA_PanCancer_UnwantedVariation) (2022).

## Acknowledgements

We thank P. Spellman, H. Shen, V. Wang and V. Gayevskiy for helpful comments on the near-final draft. Thanks to the TCGA Research Network for generating the data used in this study and to groups who have made the raw and normalized datasets publicly

available. R.M. and A.T.P. were supported by the Lorenzo and Pamela Galli Medical Research Trust. R.M. was supported by funding from the Ovarian Cancer Research Foundation. A.T.P. was supported by an Australian National Health and Medical Research Council (NHMRC) Senior Research Fellowship (1116955). M.F. was funded by a Prostate Cancer Foundation Young Investigator Award. A.D. was funded for this work by a National Breast Cancer Foundation grant (II-RS-19-108). The research benefitted by support from the Victorian State Government Operational Infrastructure Support and Australian Government NHMRC Independent Research Institute Infrastructure Support.

### Author contributions

R.M., A.D., A.T.P. and T.P.S. designed the overall approach. R.M., J.G.B., G.O. and T.P.S. developed the pseudo-replicate of pseudo-samples approach. R.M., M.F. and L.G. performed data analysis. A.J., R.M. and M.F. developed the RShiny application. A.S., R.M. and M.F. developed the R package tcgaCleanR. R.M., M.F., A.T.P. and T.P.S. wrote the manuscript, which was revised and approved by all authors.

### Competing interests

The authors declare no competing interests.

### Additional information

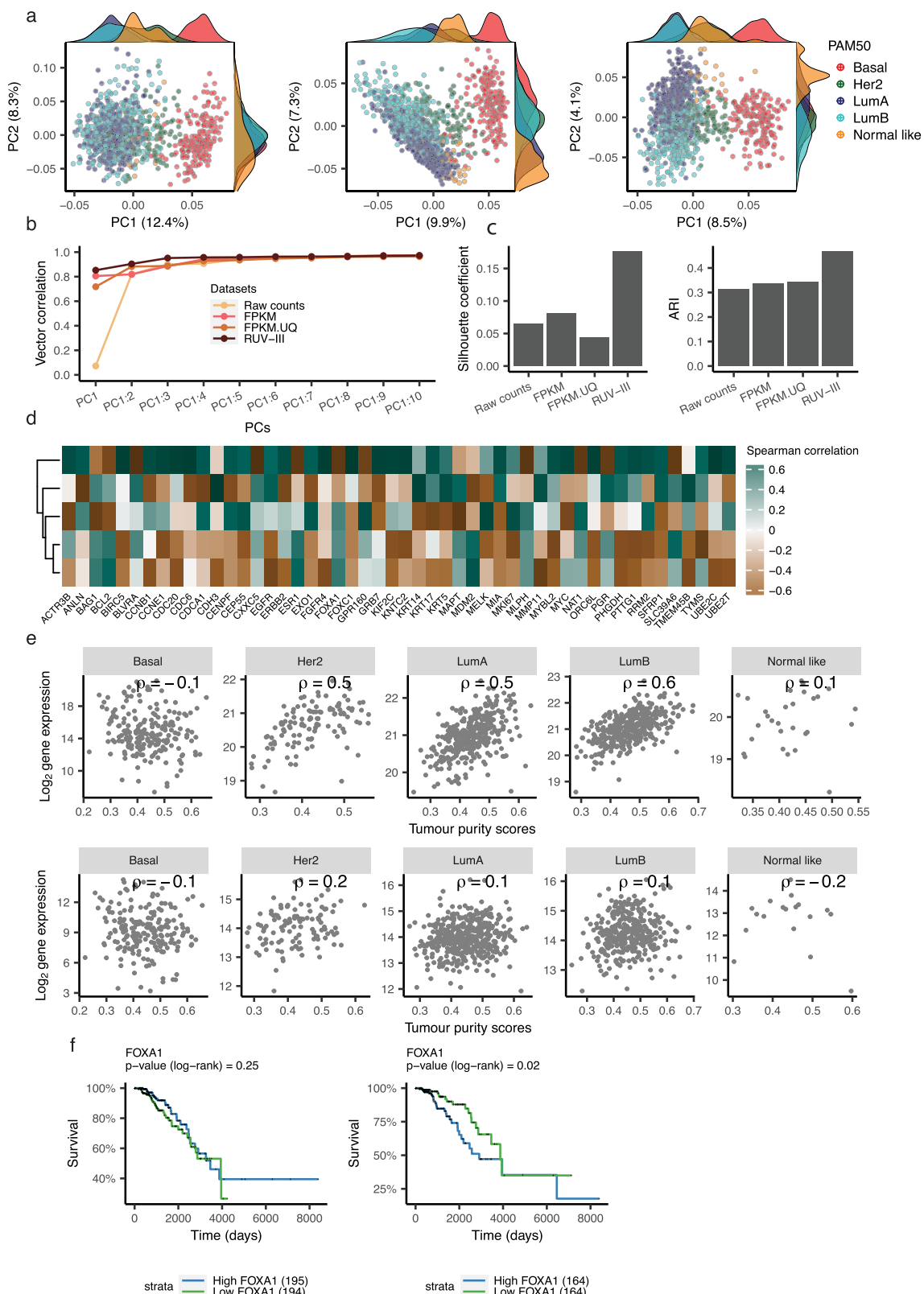
**Extended data** is available for this paper at <https://doi.org/10.1038/s41587-022-01440-w>.

**Supplementary information** The online version contains supplementary material available at <https://doi.org/10.1038/s41587-022-01440-w>.

**Correspondence and requests for materials** should be addressed to Ramyar Molania, Anthony T. Papenfuss or Terence P. Speed.

**Peer review information** *Nature Biotechnology* thanks Olivier Gevaert, Arjun Bhattacharya and the other, anonymous, reviewer(s) for their contribution to the peer review of this work.

**Reprints and permissions information** is available at [www.nature.com/reprints](http://www.nature.com/reprints).



**Extended Data Fig. 1 | See next page for caption.**

**Extended Data Fig. 1 | RUV-III improves the PAM50 clusters in the TCGA BRCA RNA-seq data.** **a)** Scatter plot of the first two principal components colored by the PAM50 subtypes in the FPKM (left), FPKM.UQ (middle), and the RUV-III (right) normalized datasets. **b)** Vector correlation analysis between the first ten principal components cumulatively and the PAM50 subtypes in the differently normalized datasets. **c)** Silhouette coefficients and ARI showing how the PAM50 clusters are separated in the differently normalized datasets. **d)** The heatmap gives the Spearman correlation coefficients between the expression levels of the PAM50 signature genes and the tumor purity scores in the FPKM.UQ data. **e)** Scatter plots show relationship between the gene expression levels of FOXA1 and tumor purity within the individual PAM50 subtypes in the FPKM.UQ (first row) and the RUV-III normalized data (second row). **f)** Kaplan Meier survival analyses for samples with low and high expression of FOXA1 gene in Luminal-B subtype in the FPKM.UQ (left) and the RUV-III normalized data (right).

## Unwanted variation identification (UVI)

## Known sources of UV

## I - library size (LS) and tumor purity (TP)

- o Linear regression between the first 5-10 PCs cumulatively and LS and TP separately
  - no or weak associations is desirable
- o Spearman correlation between individual gene expression and LS and TP separately
  - no or weak correlations is desirable
- o Differential gene expression analysis between samples with low and high LS and TP separately
  - a uniformly distributed p-histograms is desirable

## II - batch effects

- o PCA plots colored by known batches
  - no clusters driven by batches is desirable
- o Vector correlation between the first 5-10 PCs cumulatively and batch effects
  - no or weak associations is desirable
- o Differential gene expression analysis or ANOVA between samples from different batches
  - a uniformly distributed p-histograms is desirable
- o Relative gene expression (RLE) plot
  - medians should center around zero, boxes should be similarly sized
  - no or weak correlation between individual gene expression and the RLE medians
- **Note:** in situations where biological factors of interests are largely confounded by batches. We recommend to perform the steps above on a large publicly available housekeeping gene set (negative control genes). The majority of these genes should not be affected.

## Unknown sources of UV

## I - negative control genes

- Usually, these sources of unwanted variation can be found using a reasonably large publicly available housekeeping gene set (negative control genes).
- o Scatter plots of the first 3 PCs
    - explore distinct clusters
  - o Vector correlation between the first 5-10 PCs cumulatively and the distinct clusters
    - no or weak associations is desirable
  - o Differential gene expression analysis or ANOVA between samples form the distinct clusters
    - a uniformly distributed p-histograms is desirable

**Note:** Usually, a subset of genes are affected by unwanted variation. Then, using publicly available housekeeping genes may not reveal all unknown sources of UV, if these genes are not affected.

## II - the RLE medians

- o Perform unsupervised clustering of the RLE medians. Clusters are potentially batches.
  - perform Step II of the UVI procedure

**Note:** We recommend exploring known biology e.g. gene-gene correlations on an independent data set to see possible effects of unknown sources of UV.

## RUV-III-PRPS normalization

## Step 1: UVI

Follow the UVI procedure to find all sources of UV (call them 'batches')

## Step2: PRPS

- o If biological labels for the samples are roughly known
  - explore how biological populations are distributed across batches
  - if a biological population presents across all batches, you can generate PRPS
- o If biological labels of samples are unknown
  - roughly identify major biological populations and follow the above step

**Note:** If the identification of major biological populations is not possible, we recommend to create PRPS per batches (average all samples per batch to create a pseudo-sample) and assess the performance using the step 1 of UVI.

## Step3: Negative control genes

- o Using publicly available housekeeping genes as negative control genes (NCG)
  - perform PCA on NCG and explore how well they capture the batches identified in Step1
- o If publicly available housekeeping gene do not capture the UV identified in Step1
  - perform DE or ANOVA between biological populations
  - perform DE or ANOVA between batches
  - select the top ~ 1000 genes that are not highly affected by biological variation, but are affected by batches. use these genes as NCG

## Step4: Performance assessments

- o Perform all the steps in the UVI procedure
- o Silhouette coefficient analysis,
- o Adjusted Rand index,
- o Explore known biology (positive controls) e.g. subtype clustering, gene-gene correlation.

**Extended Data Fig. 2 | RUV-III with PRPS workflow.** Workflow to identify known and unknown sources of unwanted variation, and apply RUV-III with PRPS normalization to RNA-seq data.

## Reporting Summary

Nature Research wishes to improve the reproducibility of the work that we publish. This form provides structure for consistency and transparency in reporting. For further information on Nature Research policies, see our [Editorial Policies](#) and the [Editorial Policy Checklist](#).

### Statistics

For all statistical analyses, confirm that the following items are present in the figure legend, table legend, main text, or Methods section.

n/a Confirmed

- The exact sample size ( $n$ ) for each experimental group/condition, given as a discrete number and unit of measurement
- A statement on whether measurements were taken from distinct samples or whether the same sample was measured repeatedly
- The statistical test(s) used AND whether they are one- or two-sided  
*Only common tests should be described solely by name; describe more complex techniques in the Methods section.*
- A description of all covariates tested
- A description of any assumptions or corrections, such as tests of normality and adjustment for multiple comparisons
- A full description of the statistical parameters including central tendency (e.g. means) or other basic estimates (e.g. regression coefficient) AND variation (e.g. standard deviation) or associated estimates of uncertainty (e.g. confidence intervals)
- For null hypothesis testing, the test statistic (e.g.  $F$ ,  $t$ ,  $r$ ) with confidence intervals, effect sizes, degrees of freedom and  $P$  value noted  
*Give  $P$  values as exact values whenever suitable.*
- For Bayesian analysis, information on the choice of priors and Markov chain Monte Carlo settings
- For hierarchical and complex designs, identification of the appropriate level for tests and full reporting of outcomes
- Estimates of effect sizes (e.g. Cohen's  $d$ , Pearson's  $r$ ), indicating how they were calculated

*Our web collection on [statistics for biologists](#) contains articles on many of the points above.*

### Software and code

Policy information about [availability of computer code](#)

Data collection

NA

Data analysis

The R code of the RUV-III-PRPS method is available on this GitHub ([https://github.com/RMolania/TCGA\\_PanCancer\\_UnwantedVariation](https://github.com/RMolania/TCGA_PanCancer_UnwantedVariation)). We also provided several vignettes to reproduce all the results and figures in the paper. The Rshiny and R packag apps are also available on the GitHub page. The other statistical analyses such as PCA, RLE, ANOVA, ... were performed using both built-in functions in R version 4.1.1 and publicly available R packages as follow. The R/Bioconductor packages: biomaRt (version 2.48.3), singscore version (1.12.0), EDASEq (version 2.26.1), genefu (version 2.26.0) and the R CRAN packages: ppcor (version 1.1), cluster (version 2.1.2) and CMScallerversion 2.0.1 were used. We described all the functions and packages in full details in the manuscript.

For manuscripts utilizing custom algorithms or software that are central to the research but not yet described in published literature, software must be made available to editors and reviewers. We strongly encourage code deposition in a community repository (e.g. GitHub). See the Nature Research [guidelines for submitting code & software](#) for further information.

### Data

Policy information about [availability of data](#)

All manuscripts must include a [data availability statement](#). This statement should provide the following information, where applicable:

- Accession codes, unique identifiers, or web links for publicly available datasets
- A list of figures that have associated raw data
- A description of any restrictions on data availability

The TCGA RNA-seq data are publicly available in three formats: raw counts, FPKM and FPKM with upper-quartile normalization (FPKM.UQ). All these formats for individual cancer types (33 cancer types, ~ 11,000 samples) were downloaded using the R/Bioconductor package TCGAbiolinks (version 2.16.1). We have created summarized experiment objects containing expression data (raw counts, FPKM and FPKM.UQ), clinical and batch information, and gene annotations for all the TCGA

RNA-Seq data. These files are deposited here (<https://zenodo.org/record/6326542#.YIN56y8Rquo>). The TCGA microarray gene expression data level 3 were downloaded from the Broad GDAC Firehose repository (<https://gdac.broadinstitute.org>), data version 2016/01/28. TCGA sample processing times were downloaded from the MD Anderson Cancer Centre TCGA Batch Effects website <https://bioinformatics.mdanderson.org/public-software/tcga-batch-effects>. The TCGA survival data were downloaded from Liu et al. study [54]. The consensus measurement of --purity estimation (CPE) were downloaded from the Aran et al. study [17]. The breast cancer laser captured microdissected (LCM) and two non-TCGA RNA-seq datasets were downloaded from the NCBI Gene Expression Omnibus with accession numbers GSE78958 [37], GSE96058 and GSE81538 [49, 50] using the GEOQuery R/Bioconductor package (version 2.62.2) from the NCBI Gene Expression Omnibus. The datasets that are required for the vignettes can be found here (<https://zenodo.org/record/6392171#.YIN6Yi8Rquo>). The RUV-III normalized data of the TCGA READ, COAD and BRCA RNA-Seq datasets are deposited (<https://zenodo.org/record/6459560#.YldJ4S8Rquo>).

## Field-specific reporting

Please select the one below that is the best fit for your research. If you are not sure, read the appropriate sections before making your selection.

Life sciences  Behavioural & social sciences  Ecological, evolutionary & environmental sciences

For a reference copy of the document with all sections, see [nature.com/documents/nr-reporting-summary-flat.pdf](https://nature.com/documents/nr-reporting-summary-flat.pdf)

## Life sciences study design

All studies must disclose on these points even when the disclosure is negative.

Sample size	We assessed the performance of our method on three large TCGA RNA-seq data and two other large breast cancer RNA-seq data. Individual dataset showed different forms of unwanted variation and complexity. Therefore, the datasets are sufficient to demonstrate the accurate performances of our method.
Data exclusions	Standard filtering were applied to remove lowly expressed genes and low quality samples. The full details can be found the method section.
Replication	All normalization methods were tested across multiple independent large-scale RNA-seq datasets.
Randomization	Our study did not involve allocating samples to experimental groups.
Blinding	Our study did not involve group allocation that requires blinding.

## Reporting for specific materials, systems and methods

We require information from authors about some types of materials, experimental systems and methods used in many studies. Here, indicate whether each material, system or method listed is relevant to your study. If you are not sure if a list item applies to your research, read the appropriate section before selecting a response.

Materials & experimental systems		Methods	
n/a	Involved in the study	n/a	Involved in the study
<input checked="" type="checkbox"/>	<input type="checkbox"/> Antibodies	<input checked="" type="checkbox"/>	<input type="checkbox"/> ChIP-seq
<input checked="" type="checkbox"/>	<input type="checkbox"/> Eukaryotic cell lines	<input checked="" type="checkbox"/>	<input type="checkbox"/> Flow cytometry
<input checked="" type="checkbox"/>	<input type="checkbox"/> Palaeontology and archaeology	<input checked="" type="checkbox"/>	<input type="checkbox"/> MRI-based neuroimaging
<input checked="" type="checkbox"/>	<input type="checkbox"/> Animals and other organisms		
<input checked="" type="checkbox"/>	<input type="checkbox"/> Human research participants		
<input checked="" type="checkbox"/>	<input type="checkbox"/> Clinical data		
<input checked="" type="checkbox"/>	<input type="checkbox"/> Dual use research of concern		